Response to Referee #3

Dear reviewer,

We all appreciate the useful and revealing questions you have come up with. In this response, we try our best to answer these questions one by one. Firstly, following some previous works, we use several different methods to category the regime of turbulence during the main PM dissipation periods, including the heat flux (i.e. Van de Wiel et al., 2003 and many other works), the stability z/L by Mahrt et al. (1998), the threshold of minimum wind speed (Sun et al., 2012; Van de Wiel et al., 2012), and the statistical index (Vindel et al., 2008), revealing a very stable boundary layer and intermittent turbulence on the nights of PM dissipation. Next, we investigate the vertical transport of turbulence, finding that the strong turbulence is generated and transported from the layers above the 255-m tower, which verifies the role that the LLJ plays in the generation of turbulence and further validates the nature of intermittency of turbulence in the ABL. Finally, following your comments, we have removed the part about the radiative effects by pollutants which is irrelevant to the main topic of this work and cannot be fully proved using the available data. The detailed explanations are as follows:

The authors responded my comments carefully. In the authors' response, they further demonstrated non-stationarity of turbulence from their turbulent period (TS). Now I am totally confused.

The authors repeated the conventional understanding that intermittent turbulence is associated with stable conditions (P. 6, L18), but their intermittent turbulence index IF suggests large intermittent turbulence is during the weak stable period (TS) where turbulence is strong. That is, their definition of turbulence intermittency is opposite from those in the literature even though they claimed their intermittency index is consistent with others. It seems to me that what the authors captured is the magnitude of w fluctuations, which should be large when turbulence is strong, but that is not what turbulence intermittency supposes to mean. Turbulence intermittency means the magnitude of turbulent fluxes varies significantly not individual wind components. Wind components can fluctuate significantly but turbulent fluxes do not so that turbulent intermittency is zero. Basically what the authors show is turbulent mixing contributes to vertical dispersion of PM2.5, strong turbulence should be associated with large u*, and weak PM2.5. This is what we understand already. No wonder the authors claimed intermittent turbulence contributes to vertical dispersion of PM2.5. The authors' concept of turbulent intermittency is completely wrong.

Response: In this part, the referee pointed out two questions. One is whether the dissipation periods with large abstract values of IF can be categorized as the weakly stable condition or the very stable condition. The other is the variable used (i.e. vertical wind speed w) to evaluate the intermittency. These two questions are related with each other, so we will explain them alternatively. Also, to fully address these questions, we will focus on the periods

during which the pollutant concentration changed significantly. According to the distribution of $PM_{2.5}$ concentration in Fig. 2 in the manuscript, the decrease of pollutant concentration mainly happened during the late night to the early morning. Hence, we pay our attention to the behavior of turbulence during these periods, that is, 00:00–00:06 (LS, local time) on 27, Dec, 2016 and on 26 and 29, Jan, 2017. In the following response, all of the samples are taken from 00:00–00:06 LS unless stated otherwise.

Considering the major point of this work, we need to first specify the definition of intermittency in the ABL. According the Glossary of Meteorology (Glickman 2000), the intermittency is define as "the property of turbulence within one air mass that occurs at some times and some places and does not occur at intervening times or places". In the real works, turbulence intermittency is commonly expressed as brief episodes of turbulence with intervening periods of relatively weak or unmeasurably small fluctuations (Mahrt, 1989, 1999; Van de Wiel et al., 2002; Dadic et al., 2013) or as "bursts" vividly (Mahrt, 1999; Coulter and Doran 2002; Ohya et al., 2008). In all, intermittency is an intrinsic feature of turbulence in strongly stratified flow (Mahrt, 2006) and can be manifested by a variety of variables. As the referee suggested in the previous comments, plenty of studies sought to characterize intermittency in terms of intermittent heat flux (Howell and Sun, 1999; Coulter et al., 2002; Van de Wiel et al., 2003; Doran, 2004; Steeneveld et al., 2006; Drüe et al., 2007). Meanwhile, a number of other studies tended to define turbulent intermittency by means of wind components and even temperature. For example, Sun et al. (2002) used fluctuation of vertical wind speed w and temperature T to show intermittent turbulence periods (in their Fig. 2 and 3). In the wind tunnel experiment, Ohya et al., (2008) produced the intermittent turbulence in the SBL and showed that both the horizontal/vertical wind speed and temperature captured significant turbulent intermittency. Based on the temperature observation, Lundquist (2003) verified that Hilbert-Huang transform technique is useful for exploring intermittent events in the midlatitude atmospheric boundary layer. Some other works using wind component or temperature include Muschinski et al. (2004), Salmond and Mckendry (2005) and Vindel et al. (2008), to name just a few. Sun et al. (2012) categorized different turbulence regimes with the help of turbulence strength ($\sqrt{TKE}$) and the standard deviation of horizontal/vertical wind component ($\sigma_{V/w}$) and revealed that under the influence of non-turbulence motions, the characteristics of intermittency were manifested by different variables, including horizontal/vertical wind speed, temperature and wind direction (see their Fig. 12 and 14). In the works of Reina et al. (2004) and Mahrt et al. (2013), the variance and standard deviation of vertical wind component were applied to define the onset of intermittent turbulence events. According the works summarized above, we believe that it is justified to investigate the behavior of turbulent intermittency by means of vertical wind component w in the present study.

In literature, there are mainly two kinds of methods to classify the SBL. One way uses the so-called internal system parameters (i.e. z/L, z/Λ and so on) to define the different SBL regimes. Using the stability function z/L,

Mahrt et al. (1998) suggested three regimes: a) the weakly stable regime, b) the intermediate regime with $z/L > O(0.1)$, c) the very stable regime where $z/L > O(1)$. Although the specific threshold value of z/L depends on the level of the observations, z/L under weakly stable condition should be way less than 1, that is $0 < z/L << 1$, to keep the continuous turbulence near the surface. From the distribution of z/L in Fig. 2 in the manuscript, it can be seen that the values of z/L during the night of 26–27 Dec, 25–26 and 28–29 Jan are much larger than $O(1)$, implying very stable case during these nights. Another thing that should be clarified here is that the small mean and standard deviation of z/L during the TS in Table 2 is attributed to the extremely small z/L values at the end of the case, such as the night of 27–28 Dec and 29–30 Jan. Corresponding to the internal system parameters, the other common way to express the different SBL regimes is by using the external forcing parameters such as pressure gradient and cloud cover. A series of works by Van de Wiel et al. (2002a; 2002b; 2003) divided the SBL into turbulence case, intermittent case and radiative case in terms of a dimensionless number (Π) composited from the external forcing parameters. In their works the turbulent heat flux is chosen as indicator, because the turbulent heat flux is directly influenced by two external key parameters: the synoptic pressure gradient and the isothermal net radiation (Van de Wiel et al., 2003). The weakest stable case is characterized by continuously large sensible heat flux and for the intermittent case, turbulent and quiet periods alternate irregularly (see Fig. A2 in Van de Wiel et al., 2003). Figure 1 below shows the distribution of sensible heat flux at 40 m during three nights (26–27 Dec, 25–26 and 28–29 Jan). In order to maintain continuity, the early night (that is, 20:00–00:00) is also involved in Figure 1. Figure 1a and b show clear alternate occurrence of strong and weak flux, albeit Figure 1c is not so typical, suggesting intermittent sensible heat flux in the SBL.

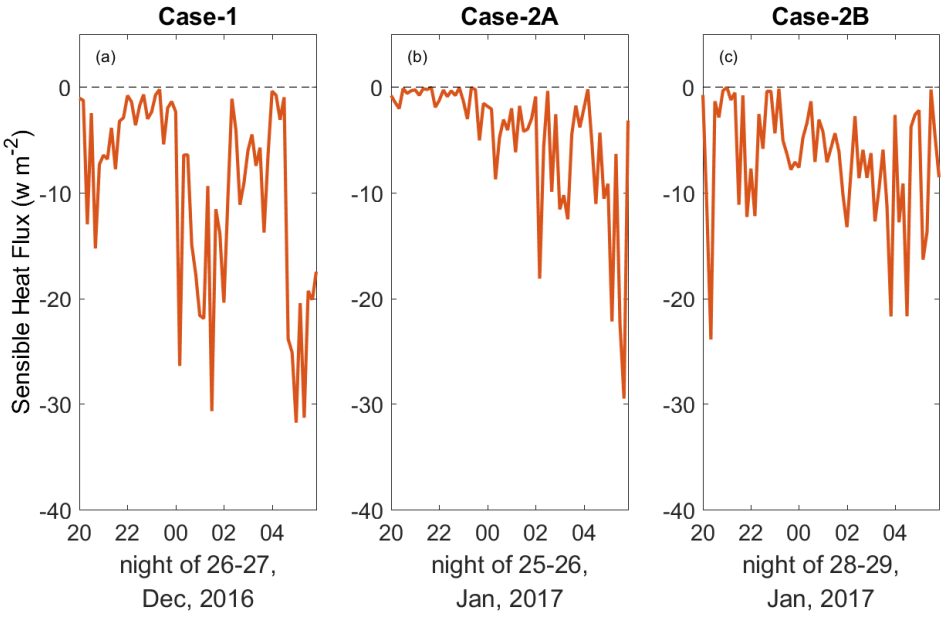

Figure 1. Time series of the sensible heat flux during the nighttime of 26–27 Dec, 25–26 and 28–29 Jan.

In addition, Van de Wiel et al. (2012) and Sun et al. (2012) revealed the relationship between turbulence strength and horizontal wind speed in different stable regimes. They found that the turbulence increases slowly with increasing wind speed under a given wind speed value, and once across the threshold value, the turbulence strengthens significantly with the increase of wind speed. And this threshold value of wind speed represents the minimum wind speed needed to sustain continuous turbulence. For the case of 40 m, the minimum wind speed for the maintenance of continuous turbulence is proposed as 5 m/s. Here we briefly introduce the theory and details can refer to Van de Wiel et al. (2012). First, it is known that the high-level winds (say, > 100 m) accelerate during the nighttime while the low-level winds (say, < 20 m) weaken in the meanwhile. Hence, the wind speed at intermediate levels (say, about 30–60 m) tends to keep constant, which follows the momentum conservation principles. Mathematically, the threshold wind speed can be seen as a velocity boundary condition for the maintenance of continuous turbulence. First, we checked the distribution of 10-min averaged horizontal wind speed V at 40 m for both two cases (Figure 2). Given that all of the values of V from the pollution cases (blue solid line) are less than 5 m/s, the extra data on 22 Dec and 22 Jan are also presented for comparison (orange solid line). From Figure 2 we can see that the nighttime horizontal wind speed V during the pollution cases (blue solid line) is generally less than 5 m/s while the values of V for normal nights (orange solid line) are larger than 5 m/s. Following the analyses of Van de Wiel et al. (2012) and Sun et al. (2012), we chose the friction velocity u_*, the

turbulence velocity scale $V_{TKE} = \sqrt{(\sigma_u^2 + \sigma_v^2 + \sigma_w^2)/2} = \sqrt{TKE}$ (define by Sun et al., 2012), and the standard deviation of the vertical speed σ_w to investigate the evolvement of turbulence with the increasing horizontal wind speed. Figure 3 gives the relationship between $u_*/V_{TKE}/\sigma_w$ and horizontal wind speed V during the nighttime. The relationship is similar between variables but shows two different patterns of evolvement within the wind speed range. In the case of pollution periods (blue), the horizontal wind speed is weak, accompanied by a slight increase of turbulence variables ($u_*/V_{TKE}/\sigma_w$) with the stronger wind speed. Once the non-pollution periods (22 Dec and 22 Jan, orange) involved, turbulence strengthens rapidly with the increasing wind speed. This abrupt transform happens when the wind speed exceeds around 4 m/s which is out of the main wind-speed range that pollution samples dominate. According to Sun et al. (2012), the strong wind range (orange) in Figure 3 corresponds to their regime-2, while the weak wind part (blue) represents the regime-1 or regime-3. Whether it falls into regime-1 or regime-3 depends on the existence of upper-level motions (i.e. LLJs). As is discussed further in the last response below, LLJs play a key role in the reproduce and downward transport of turbulence in the SBL. As the wind speed is correlated with the Richardson number for very stable conditions, this wind speed threshold could serve as the transition between very stable and weakly stable conditions (Mahrt, 2014). At this point, we can summarize Figure 2–3 by concluding that the nighttime 40-m horizontal winds during both Case-1 and Case-2 are less than the minimum wind speed, so sustained and continuous turbulence is unlikely to occur in the SBL.

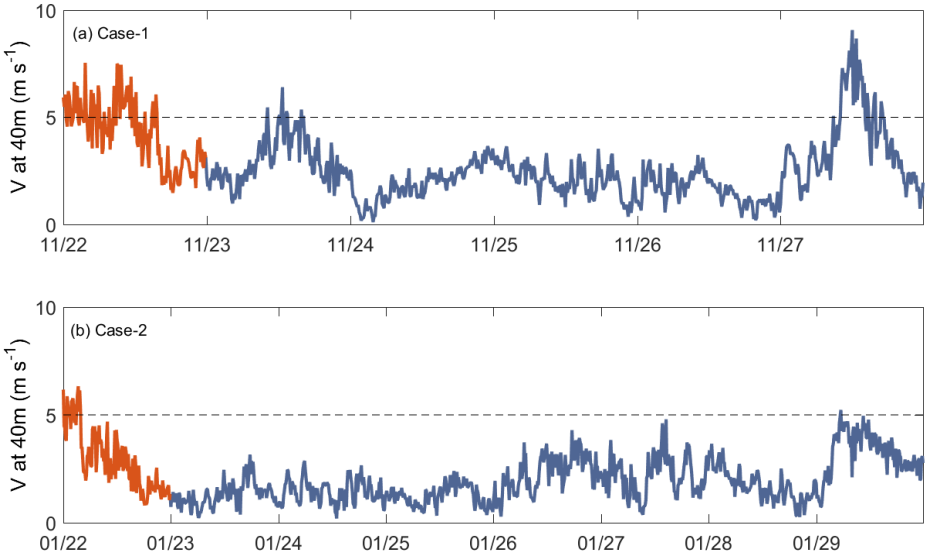

Figure 2. 10-min averaged horizontal wind speed V at 40 m for (a) Case-1 and (b) Case-2. The orange solid line represents the extra data on 22 Dec, 2016 and 22 Jan, 2017. The dashed black line marks the suggested threshold value (5 m/s).

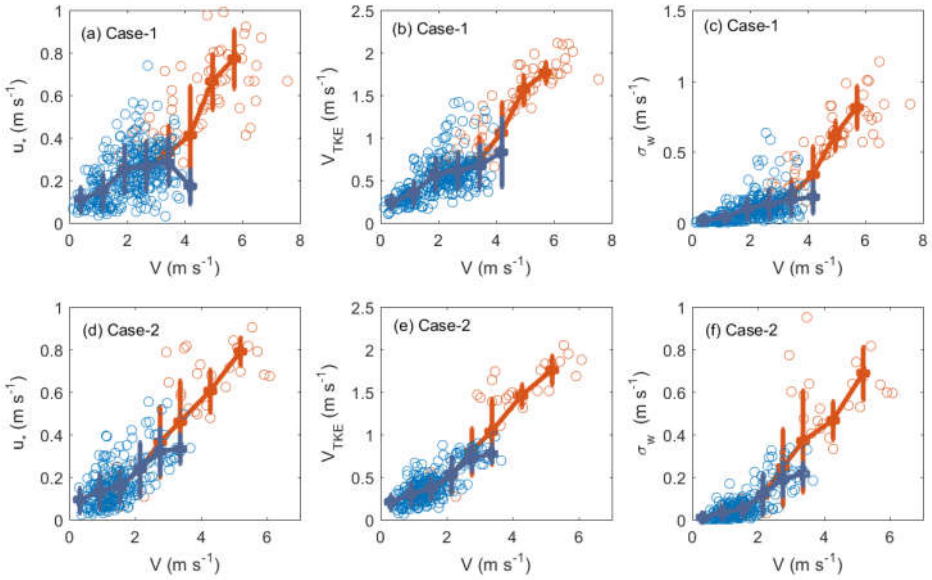

Figure 3. The relationship between the friction velocity u_*, turbulence strength V_{TKE}, standard deviation of the wind speed σ_w, and horizontal wind speed V at 40 m during the nighttime. The blue plot represents samples from the pollution cases and the orange plot is based on the extra data on the night of 22 Dec, 2016 and 22 Jan, 2017. The errorbar denotes the bin-averaged results. The top panel is for Case-1 and bottom panel is for Case-2.

As Frisch (1995) stated, when all or some of the possible symmetries are restored in a statistical sense, the turbulence at high Reynolds numbers is fully-developed. The fully-developed turbulence structure is isotropic or is the same when rotated, and the probability density function (PDF) of velocity increments should be Gaussian. However, any large-scale shearing, intermittency or strongly stable stratification in the real world could prevent symmetry restoration, resulting in a distorted PDF shape from the Gaussian form. The intermittency refers to infrequent events, which can be manifested as the velocity increments furthest from zero (Vindel et al., 2008). In this case, kurtosis can serve as a useful indicator to measure the intermittency of turbulence (Vindel et al., 2008; Mahrt 2011). Since the Gaussian distribution has a Kurtosis value of 3, it can be expected that the stronger the intermittency is, the greater the tail of PDF stretches and the larger the Kurtosis values are. Although Figure S8 in the supplement has shown the distribution of kurtosis at a scale of 10 min, Figure 4 further studies the values of Kurtosis of vertical velocity increments on different scales concentrating on the three dissipation nights. The

velocity increment is defined as $u' = u_t - u_{t+i}$ $(i = 100, 200, 300, \ldots)$, represents the fluctuation at different scales. It can be seen that for the three nights of PM dissipation, the values of Kurtosis are larger than 3 at all scales, implying that the small-scale turbulence during these periods are intermittent.

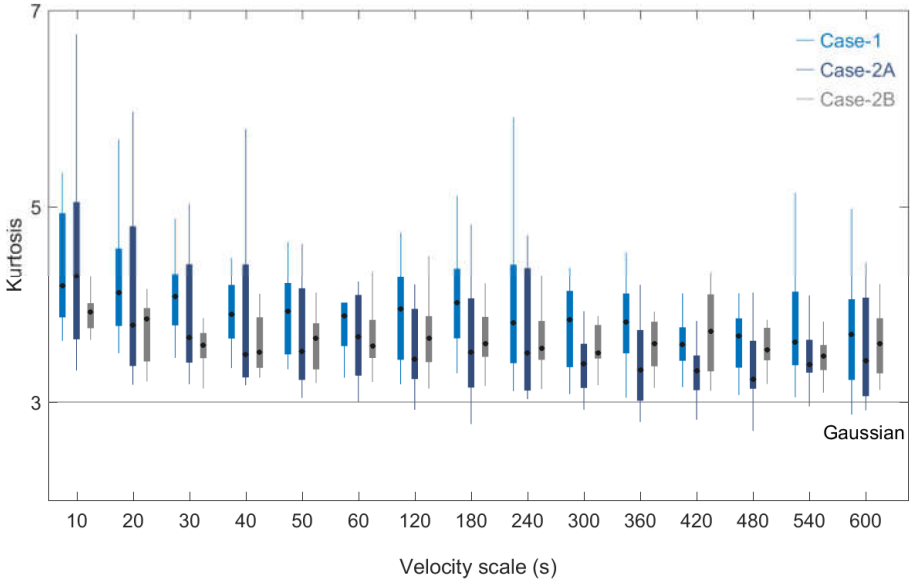

Figure 4. Kurtosis of vertical velocity increments at different scales. For each whisker diagram, the central rectangle spans the first quartile to the third quartile; the segment inside the rectangle shows the median and "whiskers" above and below the box show the locations of the minimum and maximum. The grey solid line denotes the Gaussian value.

The results above are added to the revision to help illustrate the intermittency of turbulence on the nights of PM dissipate and Figure 3–4 are attached in the supplement (see Figure S10–11). "*In terms of the horizontal wind speed, the 40-m weak wind less than the threshold value (i.e. 5 m s^{-1}) proposed by Van de Wiel et al. (2012) implies that continuous turbulence is unlikely to occur near the surface (Figure S10–11), which corresponds to the very stable turbulence regime-1 or regime-3 in Sun et al. (2012).*" (page 13, lines 6-8)

Another claim by the authors is heating at the top of the surface pollution layer by pollutants. As we know, the high pollutant concentration is highly correlated with the stable boundary layer. In other words, because of the development of the stable boundary layer, pollutants can be trapped near the surface where turbulent mixing is weak. One of the

characteristics of the stable boundary layer is air temperature increases with height. Yes, pollutants as aerosols play a role in radiative heating/cooling the atmosphere, but the authors cannot use this character of the stable boundary layer to proof the role of pollutants on radiative heating. Air temperature always increases with height in any stable boundary layer even without pollutants.

Response: Thank you for your comments. Indeed, the available results do not fully confirm the radiative effects of $PM_{2.5}$, which is also out of the scope of this work. This part has been removed from the revision.

Another claim from the authors is the role of LLJs in turbulence generation. The turbulence data used for calculating their turbulence intermittency index are at 200 m and below. The lowest wind speed measurement level from the wind profiler radar is at 200 m. All the LLJs in Fig. 9 are way above 200 m. There is no way that the authors can claim turbulence is generated way above. More likely turbulence at 200 m and below is generated by wind shear between 200 m and the surface, which is supported by the increase of wind speed at about 200 m at the beginning of the TS periods in Fig. 8.

Response: Thank you for pointing out this problem. Indeed, mere height or time distribution (as in Fig. 8 and 9 in the manuscript) cannot fully address the relationship between LLJs and turbulence, not to mention that the observation of wind profile radar (WPR) below 200 m is not available. In this part, we will try to prove that: 1) the heights of LLJ 'nose' are above the top of the tower so that the limitation of vertical observation of the WPR has little effect on the detection of LLJs; 2) with the existence of LLJs, the turbulence is transported downward at the levels across the tower, thus resulting in the so-called upside-down boundary layer; 3) and this kind of downward transported turbulence further confirms the intermittency of turbulence at lower levels. The relationship between LLJs and intermittent turbulence has been fully discussed in literature (Mahrt, 1979; 1999; 2014; Mahrt and Vickers, 2002; Balsley et al., 2003; Banta et al., 2006; Karipot et al., 2008). Under the influence of LLJs, the vertical structure of the SBL could be totally different from that of the traditional SBL. Here we cite the schematic of these two kinds of nocturnal boundary layer from Banta et al. (2006, see their Fig.1). As we know, in a traditional SBL, the turbulence is generated by the wind shear near the surface and transported upward, as shown in the top panel of Figure 5. While in the present of LLJs, the turbulence is primarily generated at upper levels of boundary layer and then transported downward to accelerate the flows near the surface, thus changing the vertical profile of a number of turbulent variables in the SBL. For example, 1) the wind shear weakens with height at lower levels and then strengthens at high levels due to the LLJ 'nose'; 2) the maximum of turbulence strength is aloft in the SBL; 3) the turbulence is transported downward and the values of vertical turbulence energy flux are negative. Based on the observation of turbulence from the tower, we can study

the vertical structure of the SBL across the tower layer. As can be seen below, although there are merely three levels observation on the tower, the basic vertical structure of the SBL is captured.

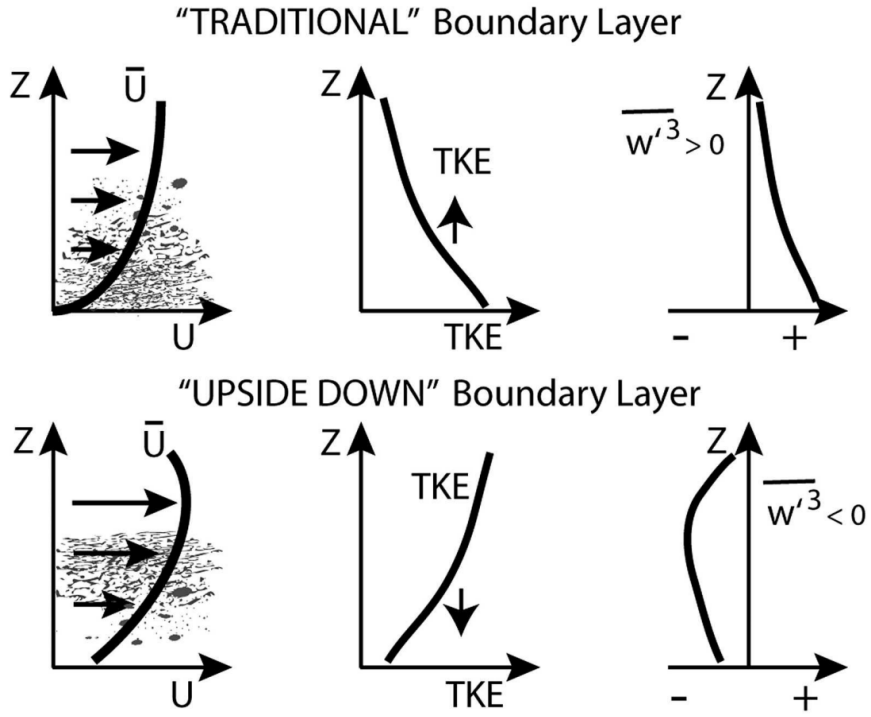

Figure 5. Schematic of structure of (top) traditional boundary layer vs (bottom) upside-down boundary layer by Banta et al. (2006), their Fig. 1. Left ones are mean horizontal wind speed profiles; center is the profiles of TKE or velocity-variance; and right ones represent the vertical turbulent transport of turbulence strength.

Figure 6–8 gives the distribution of wind shear, variance of vertical wind speed σ_w^2, and vertical transport of vertical velocity variance $\overline{w'^3}$ at different levels during three dissipation night. The early nights are also shown but the majority of information occurs after midnight. For all of the three nights, the wind shear at the lowest level is the strongest and decreases with height; the strength of turbulence enhances (σ_w^2) with height. In terms of vertical transport of turbulence energy, the values of $\overline{w'^3}$ across the tower layer are negative in Figure 6 and 7, implying the downward transport of turbulence. Although the variation of $\overline{w'^3}$ in Figure 8(i) is a bit of erratic, the majority of flux is downward to the lower layer.

In order to further study the general characteristics, the errorbar of variables at three levels is shown in Figure 9. From 40 m up to 120 m, the wind shear decreases, while the shear at 200 m increases again due to the influence of strong wind of the LLJ 'nose' (Figure. 9(a)–(c)). With respect to the variance of vertical wind speed σ_w^2, the

turbulence strength monotonously increases with height in Figure 9(d) and (f). The maximum at middle level in Figure 9(e) could be possibly attributed to the relative height of the subjet layer and the tower height, as will be discussed further below. It is known that the wind shear at the height of LLJ 'nose' is nearly zero; meanwhile, the turbulence strength of the LLJ 'nose' is weakest due to large values of Richardson number (Banta et al., 2006). Based on the vertical distribution of wind shear and turbulence strength in Figure 9(a)–(f), it can be concluded that the height of LLJ 'nose' is well above the top of the tower. A previous study on the characteristics of LLJs in Tianjin (Wei et al., 2014) revealed that there are two major height for the occurrence of LLJs in this region: one is at 250–400 m and the other is from 1,000 to 1,300 m (see their Fig. 5(d)). At this point, we can conclude that although the observation of WPR below 200 m is not available in the present study, the detection of the LLJ 'nose' in Fig. 8 and 9 of the manuscript is uninterrupted and credible.

The primary difference between a traditional SBL and an upside-down SBL is the direction of turbulence transport. It can be seen from Figure 9(g)–(i) that the value of the vertical transport of turbulence energy $\overline{w'^3}$ are negative across the tower layer, which means the turbulence is generated at higher levels and then transported downward. Besides, although the vertical transport of turbulence energy at all three nights are downward on the average, the vertical structure varies from case to case. The magnitude of $\overline{w'^3}$ for Case-2A (Figure 9h) increases from 40 m to 120 m but then decreases again when it comes to higher layer, implying a divergence layer of the downward transport of turbulence energy between 120 m and the top of the tower, which suggests that this layer corresponds to the main source of the turbulence in the subjet layer (Mahrt and Vickers, 2002). Additionally, the maximum of velocity variance σ_w^2 at 120 m in Figure 9(e) also confirms that the upper half of the tower is part of the subjet layer (Banta et al., 2006). As for Case-1 in Figure 9(g), the magnitude of the vertical transport of turbulence energy monotonously decreases with height across the tower layer and so does the velocity variance σ_w^2, suggesting that the entire tower layer is below the subjet layer in this case. The relative height of the LLJ and the tower is illustrated in the schematic in Figure 10. As for Case-2B, it is similar to Case-2A but not so typical. From its vertical transport of turbulence energy at 40 m (Figure 8(i)), we can see that upward and downward flux occur alternately, implying that the surface wind shear also plays a role in the enhancement of turbulence in the lower layer. But the negative mean values at three levels in Figure 9(i) indicate that the LLJ-generated turbulence dominates overall.

The LLJ-induced turbulence in the SBL further confirms the results about the turbulent intermittency in the first response. As mentioned above in Figure 3, the weak wind during the cases in the present study corresponds to the noncontinuous turbulence regime of Van de Wiel et al. (2012) or regime-1/regime-3 in Sun et al. (2012). The difference between regime-1 and regime-3 depends on whether a LLJ exists or not. In an upside-down SBL with

the present of LLJs, the turbulence intermittency can be classified as the category C turbulence intermittency brought up by Sun et al. (2012).

The mechanism of LLJ-generated intermittent turbulence is addressed in the revision and Figure 9 is added to the manuscript (see Fig. 10). "*It is well-known that LLJs are an important source of intermittent turbulence in the ABL, resulting in an 'upside-down' boundary layer structure (Mahrt, 1999; 2014; Poulos et al., 2002; Mahrt and Vickers, 2002; Banta et al., 2006; Balsley et al., 2003; Karipot et al., 2008). The vertical 'nose' shape of LLJs provides wind shear at upper levels, working as an elevated source of turbulent mixing. Then this turbulence is transported downward to the surface, resulting in non-stationary increase of turbulent mixing at lower levels. In this case, the vertical structure of 'upside-down' boundary layer is totally different from that of a traditional boundary layer. For example, (a) the wind shear decreases with height first and then increases again due to the LLJ 'nose' at upper levels; (b) the strongest turbulence is not at the surface but aloft; (c) the transport of turbulence energy is downward. Fig. 10 presents the vertical turbulence structure across the tower layer for three dissipation nights, during which LLJs occurred. From Fig. 10a–b, it can be seen that the wind shear weakens in the layer between 40 and 120 m; then it increases when it comes to higher levels. In terms of the variance of vertical wind speed* σ_w^2 *(Fig. 10d–f), the maximal value of turbulence strength is aloft rather than near the surface for all three nights, implying a turbulence source in mid-air. The vertical distribution of transport of turbulence energy further confirms the uplift of turbulence source. The values of the vertical transport of vertical velocity variance* $\overline{w'^3}$ *at three levels are negative generally, which means that the transport of turbulence energy across the tower layer is downward. It should be noticed that the magnitude of* $\overline{w'^3}$ *in Fig. 10h is not monotonously with height, implying a divergence layer of the downward transport of turbulence energy between 120 m and the top of the tower, which suggests that this layer corresponds to the main source of the turbulence in the subjet layer (Mahrt and Vickers, 2002). In addition, the differences in phase and strength of intermittency at three levels in Fig. 6 also confirms that the wind shear associated with the LLJ 'nose' plays an important part in the generation and transport of turbulence in the ABL.*" (page 15, lines 14-33)

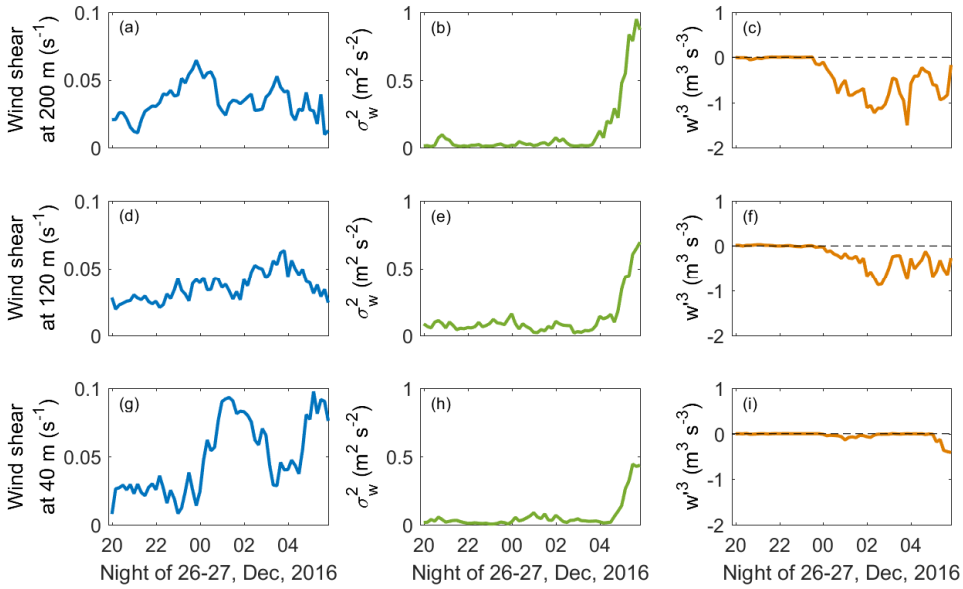

Figure 6. Distribution of wind shear, the variance of vertical wind speed σ_w^2, the vertical transport of vertical velocity variance $\overline{w'^3}$ at three levels for Case-1.

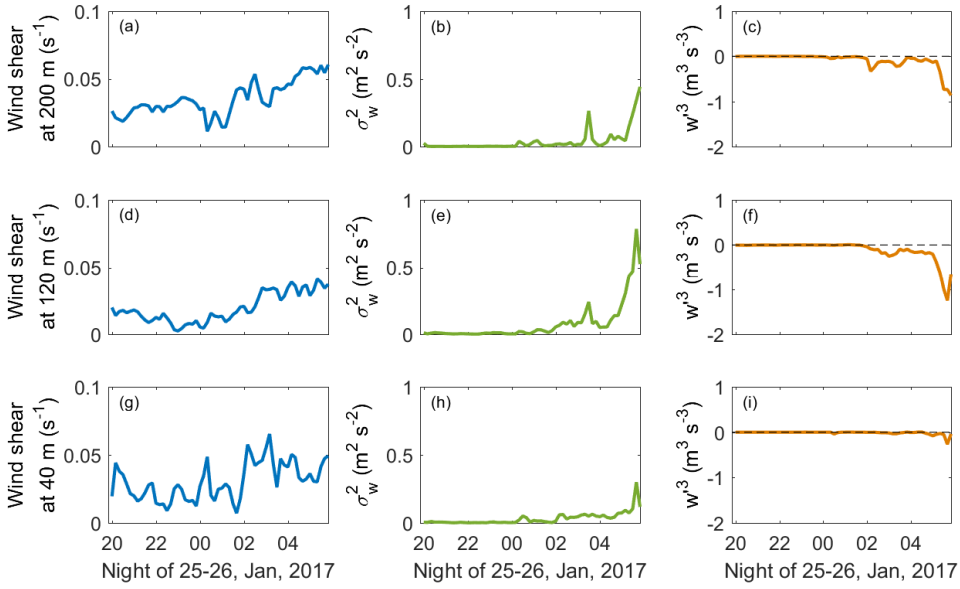

Figure 7. Same as Figure 6 but for Case-2A.

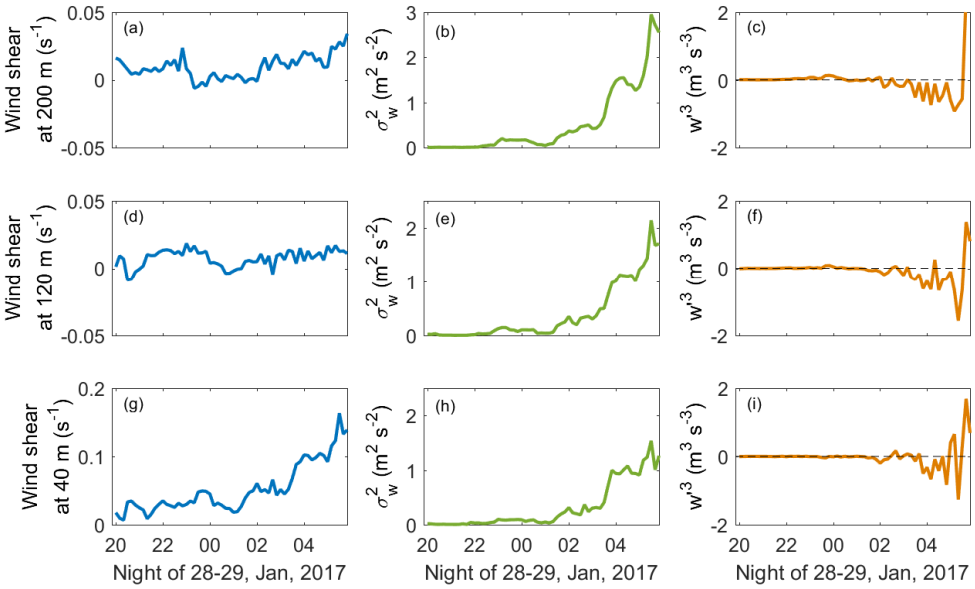

Figure 8. Same as Figure 6 but for Case-2B.

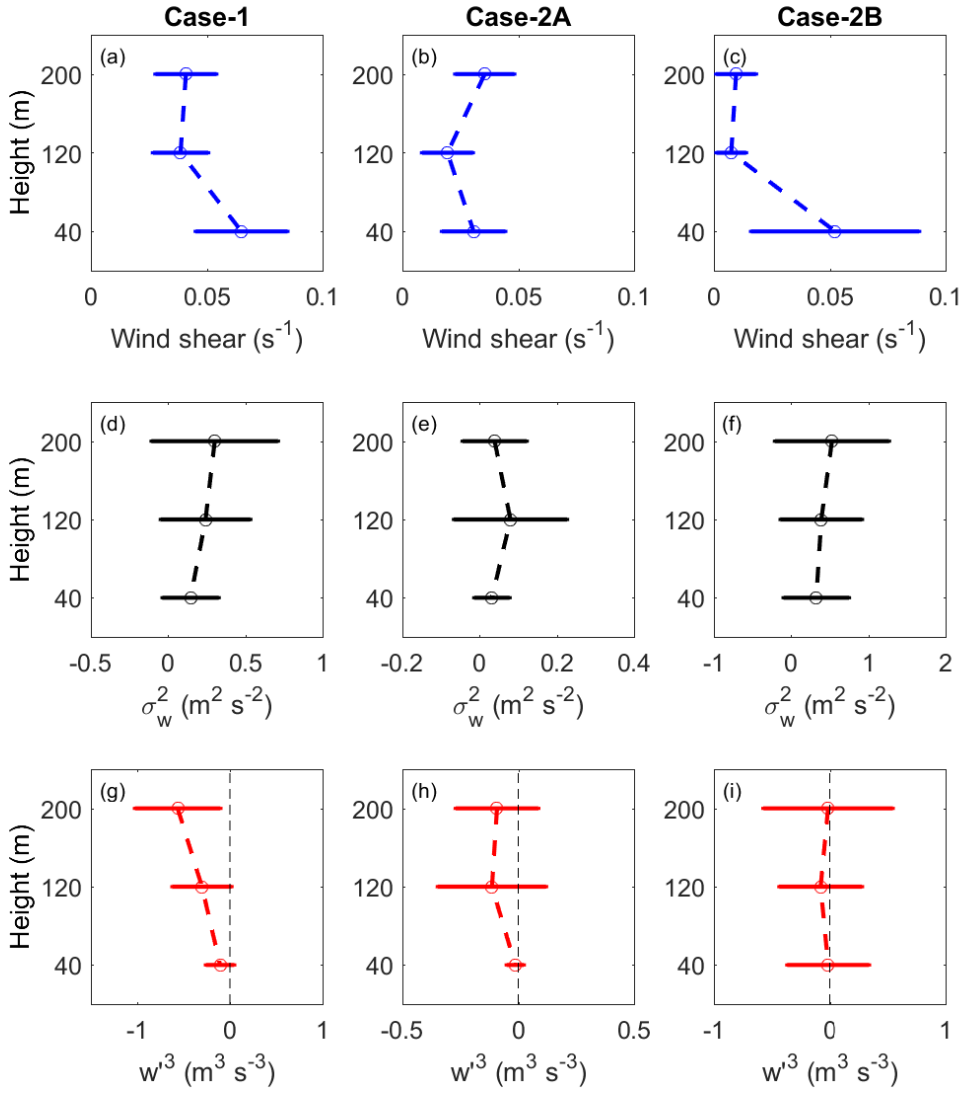

Figure 9. Vertical structure of (a–c) Wind shear, (d–f) variance of vertical wind speed σ_w^2, (g–i) vertical transport of vertical velocity variance during (left) 00:00–00:06 LS on 27, Dec, 2016; (center) 00:00–00:06 LS on 26, Jan, 2017; (right) 00:00–00:06 LS on 29, Jan, 2017. The circle of errorbar denotes the mean value and the width of bar marks the standard deviation.

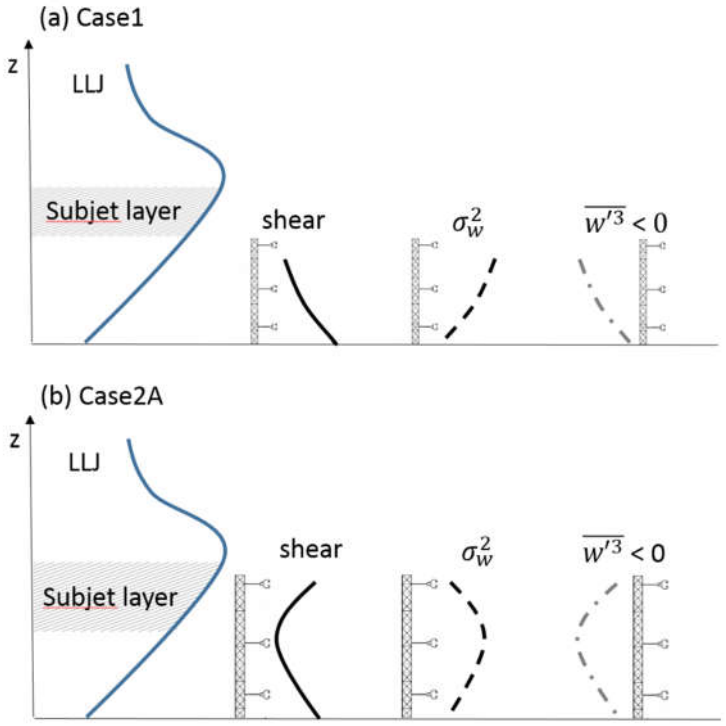

Figure 10. Schematic of the relative location of LLJ and turbulence for the night of (a) Case-1 and (b) Case-2A.

References

Balsley, B. B., Frehlich, R. G., Jensen, M. L., Meillier, Y., & Muschinski, A. (2003). Extreme gradients in the nocturnal boundary layer: Structure, evolution, and potential causes. Journal of the Atmospheric Sciences, 60(20), 2496-2508.

Banta, R. M., Pichugina, Y. L., & Brewer, W. A. (2006). Turbulent velocity-variance profiles in the stable boundary layer generated by a nocturnal low-level jet. Journal of the atmospheric sciences, 63(11), 2700-2719.

Coulter, R. L., & Doran, J. C. (2002). Spatial and temporal occurrences of intermittent turbulence during CASES-99. Boundary-layer meteorology, 105(2), 329-349.

Doran, J. C. (2004). Characteristics of intermittent turbulent temperature fluxes in stable conditions. Boundary-layer meteorology, 112(2), 241-255.

Drüe, C., & Heinemann, G. (2007). Characteristics of intermittent turbulence in the upper stable boundary layer over Greenland. Boundary-layer meteorology, 124(3), 361-381.

Frisch, U. (1995). Turbulence: the legacy of AN Kolmogorov. Cambridge University Press, Cambridge, pp 72–97.

Glickman, T. S. (2000). Glossary of Meteorology. 2nd ed. American Meteorological Society, 855 pp.

Howell, J. F., & Sun, J. (1999). Surface-layer fluxes in stable conditions. Boundary-Layer Meteorology, 90(3), 495-520.

Karipot, A., Leclerc, M. Y., Zhang, G., Lewin, K. F., Nagy, J., Hendrey, G. R., & Starr, G. (2008). Influence of nocturnal low‐level jet on turbulence structure and CO2 flux measurements over a forest canopy. Journal of Geophysical Research: Atmospheres, 113(D10).

Lundquist, J. K. (2003). Intermittent and elliptical inertial oscillations in the atmospheric boundary layer. Journal of the atmospheric sciences, 60(21), 2661-2673.

Mahrt, L. (1989). Intermittency of atmospheric turbulence. Journal of the Atmospheric Sciences, 46(1), 79-95.

Mahrt, L. (1999). Stratified atmospheric boundary layers. Boundary-Layer Meteorology, 90(3), 375-396.

Mahrt, L. (2011). The near-calm stable boundary layer. Boundary-layer meteorology, 140(3), 343-360.

Mahrt, L. (2014). Stably stratified atmospheric boundary layers. Annual Review of Fluid Mechanics, 46, 23-45.

Mahrt, L., & Vickers, D. (2002). Contrasting vertical structures of nocturnal boundary layers. Boundary-Layer Meteorology, 105(2), 351-363.

Mahrt, L., & Vickers, D. (2006). Extremely weak mixing in stable conditions. Boundary-layer meteorology, 119(1), 19-39.

Mahrt, L., Heald, R. C., Lenschow, D. H., Stankov, B. B., & Troen, I. B. (1979). An observational study of the structure of the nocturnal boundary layer. Boundary-Layer Meteorology, 17(2), 247-264.

Mahrt, L., Sun, J., Blumen, W., Delany, T., & Oncley S. (1998). Nocturnal boundary-layer regimes. Boundary-layer meteorology, 88(2), 255-278.

Mahrt, L., Thomas, C., Richardson, S., Seaman, N., Stauffer, D., & Zeeman, M. (2013). Non-stationary generation of weak turbulence for very stable and weak-wind conditions. Boundary-layer meteorology, 147(2), 179-199.

Muschinski, A., Frehlich, R. G., & Balsley, B. B. (2004). Small-scale and large-scale intermittency in the nocturnal boundary layer and the residual layer. Journal of Fluid Mechanics, 515, 319-351.

Ohya, Y., Nakamura, R., & Uchida, T. (2008). Intermittent bursting of turbulence in a stable boundary layer with low-level jet. Boundary-layer meteorology, 126(3), 349-363.

Reina, N., & Mahrt, L. (2005). A study of intermittent turbulence with cases-99 tower measurments. Boundary-layer meteorology, 114(2), 367-387.

Salmond, J. A., & McKendry, I. G. (2005). A review of turbulence in the very stable nocturnal boundary layer and its implications for air quality. Progress in Physical Geography, 29(2), 171-188.

Steeneveld, G. J., Van de Wiel, B. J. H., & Holtslag, A. A. M. (2006). Modeling the evolution of the atmospheric boundary layer coupled to the land surface for three contrasting nights in CASES-99. Journal of the atmospheric sciences, 63(3), 920-935.

Sun, J., Burns, S. P., Lenschow, D. H., Banta, R., Newsom, R., Coulter, R., ... & Blumen, W. (2002). Intermittent turbulence associated with a density current passage in the stable boundary layer. Boundary-Layer Meteorology, 105(2), 199-219.

Sun, J., Mahrt, L., Banta, R. M., & Pichugina, Y. L. (2012). Turbulence regimes and turbulence intermittency in the stable boundary layer during CASES-99. Journal of the Atmospheric Sciences, 69(1), 338-351.

Van de Wiel, B. J. H., Moene, A. F., & Jonker, H. J. J. (2012). The cessation of continuous turbulence as precursor of the very stable nocturnal boundary layer. Journal of the Atmospheric Sciences, 69(11), 3097-3115.

Van de Wiel, B. J. H., Moene, A. F., Hartogensis, O. K., De Bruin, H. A. R., & Holtslag, A. A. M. (2003). Intermittent turbulence in the stable boundary layer over land. Part III: A classification for observations during CASES-99. Journal of the atmospheric sciences, 60(20), 2509-2522.

Van de Wiel, B. J. H., Moene, A. F., Jonker, H. J. J., Baas, P., Basu, S., Donda, J. M. M., ... & Holtslag, A. A. M. (2012). The minimum wind speed for sustainable turbulence in the nocturnal boundary layer. Journal of the Atmospheric Sciences, 69(11), 3116-3127.

Van de Wiel, B. J. H., Ronda, R. J., Moene, A. F., De Bruin, H. A. R., & Holtslag, A. A. M. (2002a). Intermittent turbulence and oscillations in the stable boundary layer over land. Part I: A bulk model. Journal of the atmospheric sciences, 59(5), 942-958.

Van de Wiel, B. J. H., Moene, A. F., Ronda, R. J., De Bruin, H. A. R., & Holtslag, A. A. M. (2002b). Intermittent turbulence and oscillations in the stable boundary layer over land. Part II: A system dynamics approach. Journal of the atmospheric sciences, 59(17), 2567-2581.

Vindel, J. M., Yagüe, C., & Redondo, J. M. (2008). Structure function analysis and intermittency in the atmospheric boundary layer. Nonlinear Processes in Geophysics, 15(6), 915-929.

Wei, W., Zhang, H. S., & Ye, X. X. (2014). Comparison of low‐level jets along the north coast of China in summer. Journal of Geophysical Research: Atmospheres, 119(16), 9692-9706.

List of relevant changes in the manuscript

Change 1. The categorization of the SBL regime by the method of Van de Wiel et al. (2012) and Sun et al. (2012) is cited in the revision to illustrate the very stable condition of the SBL in the present study.

Change 2. The statement about the radiative effect of pollutants is removed from the revision.

Change 3. The vertical structure of the SBL within the tower height based on the three-level turbulence observation reveals that 1) the absent of observation below 200m of the WPR does not affect the detection of LLJ 'nose'; 2) the turbulence is generated aloft and transported downward to the surface during the periods of dissipation due to the existence of LLJs; 3) the downward transport of turbulence verifies that the turbulence in the SBL is intermittent essentially.

Marked-up manuscript version

Intermittent turbulence contributes to vertical dispersion of $PM_{2.5}$ in the North China Plain: cases from Tianjin

Wei Wei[1], Hongsheng Zhang[2], Bingui Wu[3], Yongxiang Huang[4], Xuhui Cai[5], Yu Song[5], Jianduo Li[1]

[1]State Key Laboratory of Severe Weather, Chinese Academy of Meteorological Sciences, Beijing 100081, P.R. China
[2]Laboratory for Climate and Ocean-Atmosphere Studies, Department of Atmospheric and Oceanic Sciences, School of Physics, Peking University, Beijing 100081, P.R. China
[3]Tianjin Municipal Meteorological Bureau, Tianjin 300074, P.R. China
[4]State Key Laboratory of Marine Environmental Science, Xiamen University, Xiamen 361005, P.R. China
[5]State Key Joint Laboratory of Environmental Simulation and Pollution Control, Department of Environmental Science, Peking University, Beijing 100081, P.R. China

Correspondence to: Hongsheng Zhang (hsdq@pku.edu.cn)

Abstract. Heavy particulate pollution events have frequently occurred in the North China Plain over the past decades. Due to high emissions and poor dispersion conditions, issues become increasingly serious during cold seasons. Although early studies have explored some potential reasons for air pollutions, there are few works focusing on the effects of intermittent turbulence. This paper draws upon two typical $PM_{2.5}$ (particulate matter with diameter less than 2.5 mm) pollution cases from the winter of 2016–2017. After several days of gradual accumulation, the concentration of $PM_{2.5}$ near the surface reached the maximum as a combined result of strong inversion layer, stagnant wind and high ambient humidity and then sharply decreased to a very low level within a few hours. In order to identify the strength of turbulent intermittency, an effective index, called Intermittency Factor (IF), was proposed by this work. The results show that the turbulence is very weak during the cumulative stage due to the suppression by strongly stratified layers; while for the stage of dispersion, the turbulence is highly intermittent and not locally generated. The vertical ~~characteristic~~ structure of ~~IF~~ turbulence and wind profiles confirm the generation and downward transport of intermittent turbulence ~~from the wind shear~~ associated with low-level jets. The intermittent turbulent fluxes contribute positively to the vertical transport of particulate matter and improve the air quality near the surface. This work brought up a possible mechanism of how intermittent turbulence affects the dispersion of particulate matter.

1 Introduction

In the winter of 2016–2017, severe air pollution events haunted the North China Plain, affecting more than 1/5 of the total population in China (Ren et al., 2017). Particulate pollution, especially $PM_{2.5}$ (particulate matter with diameter less than 2.5

mm) pollution, has become the foremost problem, considering its adverse impacts on human health (Dominici et al., 2014; Nel, 2005; Thompson et al., 2014; Zheng et al., 2015b).

Naturally, researchers are alarmed by these issues and want to understand the potential reasons. Some works (Wang et al., 2010; Zhang et al., 2016) reveal the effects of the increasing consumption of fossil fuel and the production of secondary pollutants. Meanwhile, it is reported that climate change (Yin et al., 2017; Yin and Wang, 2017) and synoptic circulation (Zhang et al., 2017; Miao et al., 2017; Ye et al., 2016; Zhang et al., 2012; Zheng et al., 2015a; Jiang et al., 2015) are of great importance in the transport of pollutants as well. Air pollution is essentially a phenomenon of the atmospheric boundary layer (ABL) and is strongly affected by the thermodynamic and dynamic structure of the ABL (Bressi et al., 2013; Gao et al., 2016; Tang et al., 2016). The spatial and temporal structures of turbulent motions have a dominant influence on the local air quality from the hourly scale to the diurnal scale (Shen et al., 2017). However, most of the works (Petäjä et al., 2016) focus on the feedback between aerosol, turbulent mixing and boundary layer, with little discussion on the dynamic effect of turbulence on the transport of particulate matter, not to mention the intermittent turbulence under strongly stable conditions. In fact, severe particulate pollutions tend to frequently occur in cold seasons in northern China (Sun et al., 2004; Zhang and Cao, 2015), during which the stratification of the ABL is more stable (Wang et al., 2017) and the turbulent mixing is relatively weak and intermittent in both temporal and spatial scales (Klipp and Mahrt, 2004; Mahrt, 2014). A series of works (Helgason and Pomeroy, 2012; Noone et al., 2013; Vindel and Yagüe, 2011) have confirmed that the intermittent turbulence accounts for a large amount of the vertical momentum, heat and mass exchange between the surface and the upper boundary layer, implying that intermittent turbulence may be one of the key factors in the pollutant dispersion.

The intermittency of velocity fluctuations comes in bursts (as shown in Figure 2 in Frisch, 1980), which means that turbulent intermittency is non-stationary and has no specific time scale. Moreover, the turbulence in the ABL is inherently nonlinear (Holtslag, 2015) and has complex interaction with other motions, such as low-level jets, gravity waves, solitary waves and other non-turbulence motions (Banta et al., 2006; Sun et al., 2015; Terradellas et al., 2005). To date, different methods have been applied to describe the levels of intermittency, such as the flatness (Frisch, 1995), FI index (Flux Intermittency, Eq. (9) in Mahrt, 1998), wavelet analysis (Salmond, 2005) and so on. Given the non-linearity and non-stationarity of intermittent turbulence in the ABL, we conduct our study using a new technique, the so-called arbitrary-order Hilbert spectral analysis (arbitrary-order HSA, Huang et al., 2008), which has been successfully applied into the analyses of turbulence (Huang et al., 2009, 2011; Schmitt et al., 2009; Wei et al., 2016, 2017). It should be noticed that, the target of this work is not to compare the cons and pros of different methods but to study the turbulent intermittency in the ABL with the help of an effective method. The methodology is generalized and the advances are clarified in Sect. 2.2.

Based on these considerations, this work mainly aims at:

1) quantifying the turbulent intermittency in the ABL using the arbitrary-order HSA technique;
2) revealing a possible mechanism of the dispersion of near-surface $PM_{2.5}$ from a viewpoint of intermittent turbulence.

In the following text, the data and method are introduced in Sect. 2. Then Sect. 3 discusses our results in detail, including an overview of the cases, the behavior of turbulence intermittency and its contribution to the pollutant transport. The last Sect. 4 is a conclusion.

2 Data and Method

2.1 Observation

Tianjin (39.00 °N, 117.21°E, altitude 3.4 m) is the largest coastal city in the North China Plain with a population of more than 1.5 million, covering an area of 11,300 km^2. Tianjin is located to the southeast of Beijing, the capital of China, and neighbors Bohai Sea to the east (Fig. 1). Due to the rapid urbanization in the past decades, Tianjin has a typical urban underlying terrain.

Observations in this work include three parts: 1) a 255-m meteorological observation tower for the measurement of turbulence; 2) a CFL-03 wind-profile radar (WPR) for the boundary-layer wind field; and 3) a TEOM 1405-DF system for the monitor of particular matter. The 255-m meteorological observation tower is situated in the Tianjin Municipal Meteorological Bureau, equipped with three levels (40, 120, and 200 m) of sonic anemometers (CSAT, CAMPBELL, Sci., USA) operating at a sampling frequency of 10 Hz. In addition, the observation (HMP45C, CAMPBELL, Sci., USA) at 15 levels is also used to analyze the behavior of relative humidity (RH) and temperature. The Tianjin Municipal Meteorological Bureau is located in a residential and traffic area and the buildings around the 255-m meteorological observation tower are typically 15-25 m in height (Ye et al., 2014). In order to avoid affecting the residential zone, the CFL-03 boundary-layer WPR is mounted nearly 10 km away from the Tianjin Municipal Meteorological Bureau to the west. The 1405-DF TEOM system is located nearly 2.3 km away from the 255-m tower to the east and installed at a height of 3 m to monitor the surface $PM_{2.5}$. Detailed information is listed in Table 1.

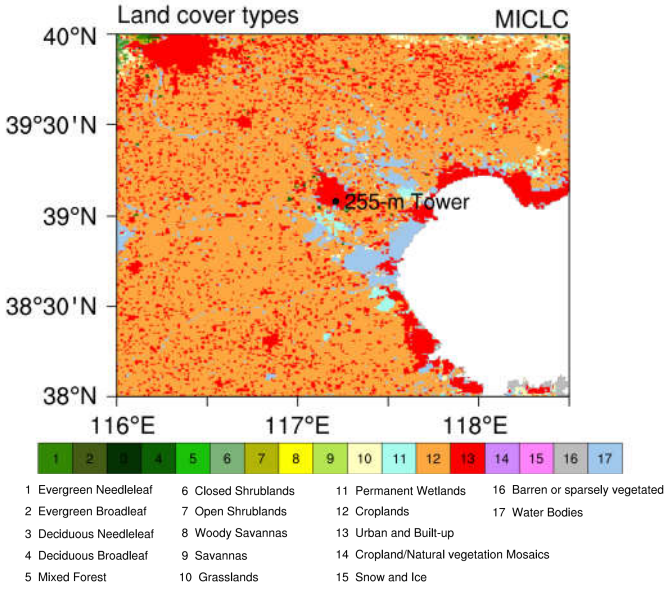

Figure 1: Landuse map around the site. The black dot denotes the location of the 255-m meteorological observation tower.

Table 1. Performance characteristics of instruments

Instrument	Height	Variables	Sampling resolution	Range	Accuracy
Sonic anemometer-thermometer, CSAT3[a]	40, 120, 200 m	3-D wind speed ($u_{x/y/z}$), Sonic virtual temperature	0.1 s	u_x, u_y: ± 65.536 m s^{-1} u_z: ± 8.192 m s^{-1} c[e]: 300–366 m s^{-1} (-50–60°C)	u_x, u_y: < ± 4 cm s^{-1} u_z: < ± 2 cm s^{-1}
HMP45C[a]	15 levels[b]	Temperature, Relative humidity	15 s	-40–60°C 0–100%	± 0.2°C ± 2% (<90%) ± 3% (>90%)
1405-DF TEOM[c]	3 m	$PM_{2.5}$	1 hr	0–1,000,000 µg m^{-3}	± 7.5%
CFL-03 boundary layer WPR[d]	< 5,000 m	Horizontal/vertical wind speed ($U_{h/v}$), wind direction	Temporal: 10 min Vertical: 100 m	U_h: 0–60 m s^{-1} U_v: ±20 m s^{-1} Direction: 0–360°	$U_{h/v}$: 0.1 m s^{-1} Direction: ≤ 10°

[a] CAMPBELL, Sci., USA
[b] 15 levels: 5, 10, 20, 30, 40, 60, 80, 100, 120, 140, 160, 180, 200, 220, and 250 m
[c] Thermo Fisher Scientific, USA
[d] China Aerospace Science & Industry Corp

[e] c is the sound of speed

Turbulence observations from the 255-m tower were obtained at a sampling frequency of 10 Hz. Then quality control was applied to all the data (Zhang et al., 2001), such as error flag, spike detection, cross wind correction, spectral loss correction, sonic virtual temperature correction, density fluctuation correction, and coordinate rotation. If more than 20% points within a given 30-min time series were detected as outliers, then this 30-min observation was discarded. An averaging time length of 1 min was applied to calculate turbulent fluctuations and fluxes, given the small size eddies under stable conditions. The friction velocity u_* reads in its form as $u_* = (\overline{u'w'}^2 + \overline{v'w'}^2)^{1/4}$, where u′/v′/w′ represent the longitude, lateral and vertical fluctuation of wind vector. The turbulent kinetic energy (TKE) is given by $\mathrm{TKE} = (\overline{u'^2} + \overline{v'^2} + \overline{w'^2})/2$ and the stability function uses $z/L = -\kappa z g\overline{w'\theta'}/\bar{\theta}u_*^3$, in which $L = -\bar{\theta}u_*^3/\kappa g\overline{w'\theta'}$ is Obukhov length, θ is potential temperature, z is observation height, g is gravitational acceleration and κ is von Karman constant with a value of 0.4 here. The data quality of CFL-03 boundary-layer WPR was checked to avoid the effects of poor quality of data. First, data below 200 m were removed due to the interference of surrounding environment, including trees and buildings. Then each vertical profile was checked through and points with larger than 2.5 standard deviations were regarded as outliers and discarded. A profile was discarded if more than 40% of the data points were outliers or missing (Wei et al., 2014).

Based on an overall consideration of data quality and severity of air quality, two cases happening in the winter of 2016–2017 were identified to study the relationship between intermittent turbulence and pollutant dispersion. The first one persisted for 5 days from 00:00 on 23 November 2016 to 00:00 on 28 November 2016, which is marked as Case-1 for convenience purposes. The second case, that is, Case-2, is from 00:00 on 23 January 2017 to 00:00 on 30 January 2017. All of the time in this work refers to Beijing Time.

2.2 Method

The flow in the ABL is highly nonlinear and non-stationary. In order to deal with the nonlinear and non-stationary time series, we adopted a relatively new technique called the arbitrary-order Hilbert spectral analysis (arbitrary-order HSA, Huang et al., 2008), which is based on the Hilbert-Huang transform (Huang et al., 1998, 1999). The primary reason why the arbitrary-order HSA is used in this work is that this method satisfies locality and adaptivity which are two necessary conditions for the study of nonlinear and non-stationary time series (Huang et al., 1998). Based on the arbitrary-order HSA, we proposed an index, called intermittency factor (IF), to quantify the level of turbulent intermittency, which is assumingly more effective compare with some classic quantities. To investigate the effects of vertical mixing in the dispersion of air pollutants, a set of vertical wind fluctuation at 10 Hz obtained by the sonic anemometers were drawn upon in this study. A brief introduction to the method is mathematically described in this part. For detailed information, one can refer to the work by Huang et al. (2008).

Firstly, a 30-min vertical wind-speed signal X(t) is separated into a group of intrinsic mode functions $C_i(t)$ and a residual $r_n(t)$ according to the so-called empirical mode decomposition. Here, each intrinsic mode functions $C_i(t)$ meets two constraints: (i) the difference between the number of local extrema and the number of zero-crossings must be zero or one, and (ii) the running mean values of upper and lower envelops are zero. The decomposition process is as follows (Huang et al., 1998, 1999):

1) The first step is to form the upper envelope $e_{max}(t)$ based on the local maxima of 30-min X(t) using the cubic spline interpolation. The lower envelope $e_{min}(t)$ can be constructed following the same method.
2) Then, one can define the mean $m_1(t) = (e_{max}(t) + e_{min}(t))/2$ and the first local signal $h_1(t) = X(t) - m_1(t)$.
3) So far, $h_1(t)$ is checked whether it meets the two constraints of intrinsic mode functions. If yes, $h_1(t)$ is the first intrinsic mode function $C_1(t) = h_1(t)$ and is taken away from X(t) to obtain the first residual $r_1(t) = \mathrm{X(t)} - C_1(t)$. Then $r_1(t)$ is treated as the new signal to begin with step 1). If $h_1(t)$ does not meet the above constraints, the first step is repeated on $h_1(t)$ to define the lower and upper envelopes and further the new local detail until $h_{1k}(t)$ is the first intrinsic mode function $C_1(t) = h_{1\mathrm{k}}(t)$.

Steps 1–3 are called 'sifting process'. To avoid over-sifting, the standard deviation criterion (Huang et al., 1998) is applied to stop this decomposition process. After n times of 'sifting process', one obtains a set of $C_i(t)$ and a monotonic residual $r_n(t)$. At this point, the vertical wind fluctuation X(t) can be expressed as $\mathrm{X(t)} = \sum_{i=1}^{n} C_i(t) + r_n(t)$. Then, each mode $C_i(t)$ is developed to obtain its corresponding analytical signal $C_i^A(\mathrm{t}) = C_i(t) + j\tilde{C}_i(t) = A_i(t)\exp(j\theta_i(t))$ using Hilbert transform (Cohen, 1995), where the imaginary part reads as $\tilde{C}_i(t) = \frac{1}{\pi}\int_{-\infty}^{\infty} \frac{C_i(\tau)}{t-\tau} d\tau \frac{d\theta_i}{dt}$, and $A_i(t)$ and $\theta_i(t)$ are the instantaneous amplitude and phase. Also, one can define the instantaneous frequency as $\omega_i(t) = \frac{1}{2\pi}\frac{d\theta_i}{dt}$.

Note that the instantaneous amplitude $A_i(t)$ and frequency $\omega_i(t)$ are both a function of time, which means that a Hilbert spectrum $\mathrm{H}(\omega, t)$ can be defined with $A_i(t)$ expressed in the space of frequency–time. So does the joint probability density function (p.d.f.) $\mathrm{p}(\omega, A)$. If $\mathrm{H}(\omega, t)$ is integrated with respect to time, one can get $\mathrm{H}(\omega)$ which can be further expressed as $\mathrm{H}(\omega) = \int \mathrm{p}(\omega, A)A^2 dA$. If the power exponent of instantaneous amplitude is extended from 2 to q, one can define arbitrary-order Hilbert spectrum as $\mathcal{L}_q(\omega) = \int \mathrm{p}(\omega, A)A^q dA$, where $\mathrm{q} \geq 0$ is the arbitrary moment.

In the case of scale invariance, the arbitrary-order Hilbert spectrum follows $\mathcal{L}_q(\omega) \sim \omega^{-\xi(q)}$ in the inertial subrange, in which ω is the frequency and $\xi(q)$ is the scaling exponent function. Under the assumption of fully developed turbulence, the distribution of scaling exponent function with the order q is linear and meets $\xi(q) - 1 = q/3$, which is developed from $\xi(q) = \zeta(q) + 1$ (Huang et al., 2008, 2011), where $\zeta(q)$ is the scaling exponent function in q–order structure function $S_q(l) = \langle(\delta X(l))^q\rangle = \langle(X(l + l_0) - X(l_0))^q\rangle \sim l^{\zeta(q)}$, in which the angular bracket refers to spatial averaging and l means distance. This exponent law is in agreement with Kolmogorov's hypothesis (K41 for short) and any intermittency would result in deviations from the theoretical $q/3$ (Basu et al., 2004). Based on this, we define an index IF as the deviation from the theoretical value at the maximal order: $\mathrm{IF} = \xi(q_{max}) - 1 - q_{max}/3$. Due to the limited observation length, the maximal

order q_{max} is up to 4 in this study to avoid the difficulties and errors in the measurements of high-order moments (Frisch, 1995).

It is well acknowledged that the intermittent turbulence under stable conditions is characterized by sporadic bursts in a timescale of order $O(10)$ to $O(1000)$ sec. The statistically unsteady turbulence disobeys the assumptions of traditional theories (Poulos et al., 2002). For example, Fourier spectral analysis asks for a linear system and strictly stationary data; and the widely used wavelet transform is suitable for non-stationary signals but suffers when it comes to nonlinear cases (Huang et al., 1998). As one of the most important steps through this method, the empirical mode decomposition separates the original time series into different modes based on its own physical characteristics without any predetermined basis, implying an intuitive, direct, adaptive, and data-based nature. And with the instantaneous information from the Hilbert transform, one can investigate the behavior of local events, which makes the Hilbert-based method more appropriate for the analyses of intermittent turbulence. This Hilbert-based scaling exponent function $\xi(q)$ has been applied into the analyses of turbulent intermittency in the ABL (Wei et al., 2016, 2017) and shown its effectiveness and validity.

3 Results and Discussion

3.1 Overview of Cases

Figure 2 illustrates the time series of different variables for two cases, including surface $PM_{2.5}$ concentration, wind vector, temperature, RH, horizontal wind speed, vertical wind speed, friction velocity u_*, TKE, and stability parameter z/L. From the distribution of $PM_{2.5}$, it can be seen that the concentration of $PM_{2.5}$ gradually increased to maxima (263 μg m^{-3} for Case-1 and 412 μg m^{-3} for Case-2) and then dropped to a low level within a few hours. Based on the concentration of $PM_{2.5}$, we can easily divide each case into two periods: one called the cumulative stage (CS) during which the particulate matter accumulates near the surface; the other named as the transport stage (TS) representing the stage when pollutants dissipate (Zhong et al., 2017). At this point, Case-1 can be separated into the CS from 00:00 on 23 November to 06:00 on 27 November 2016 and the TS from 06:00 on 27 November to 00:00 on 28 November 2016. Case-2 experienced two transitions from the CS to TS which happened at 00:00 on 26 January 2017 and at 00:00 on 29 January 2017, respectively. To distinguish these two transitions, the former is marked as Case-2A and the latter is Case-2B. Table 2 compares the values of mean and standard deviation of different variables between CSs and TSs. Generally, the mean concentration of $PM_{2.5}$ during the CS is much higher than that for the TS. For Case-1, wind at lower levels mainly comes from the south-east during the CS, while the dominant wind direction turns into west when it comes to the TS. Although the wind direction for Case-2 is seemingly unsteady in Fig. 2, the statistical the rose diagrams (see Figure ~~S8~~S7) confirm a similar result, with south-easterly flows dominating the CS and westers for the TS. This wind-direction pattern is in agreement with previous works (Zhang et al., 2017; Miao et al., 2017; Zheng et al., 2015a; Jiang et al., 2015). They found that south-easterly wind can bring the aerosols emitted by the surrounding cities to this region while the clean hours are normally characterized by strong high-

pressure centers northwest of the polluted region in winter. However, in the region with densely distributed mega-cities (as in the case of Tianjin), because the upwind flows is polluted, mere advection may not be enough to disperse pollutants, thus resulting in persistent air pollution events (Zheng et al., 2015a; Chan and Yao, 2008).

In terms of temperature, it goes through gradual increase over CSs despite of its diurnal change~~, which can be attributed to two possible reasons. On one hand, the accumulation of air pollutants results in the increase of the optical depth of the atmospheric column. The majority of incoming solar radiation during the daytime is absorbed by the upper air or scattered into different direction. The part of absorbed radiation heats the upper atmospheric layer, thus contributing positively to inversion layer which is helpful to suppress the turbulent mixing in the ABL (Petäjä et al., 2016). On the other hand, the heavily polluted ABL reduces the loss of surface longwave radiation during night, which is analogous to a cloud covered night. In this case, the heated boundary layer develops into stable stratification~~. Furthermore, Fig. 3 depicts the distribution of Planetary Boundary Layer Height (PBLH) and the daily mean potential temperature profiles at 15 different heights, including change of θ over the CS (Fig. 3a–c) / TS (Fig. 3d–f) and the development during the whole polluted event (Fig. 3g). The Δθ at given height of CSs was calculated by subtracting the value of θ on the last day from that on the first day. And so it does for TSs. For Case-1, Δθ during the CS at the lowest level (5 m) is only 5.2 K. But for the top level at 250 m, Δθ is relatively larger with a value of 6.8 K. This result confirms that the warming of upper layers is stronger than that of lower layers, implying an increasingly stably stratified boundary layer during polluted days. Figs. 3b and 3c for Case-2 verify this conclusion as well. On the contrary, Δθ during TSs (Fig. 3d–f) presents a significant cooling at higher levels, denoting the collapse of inversion layer at the end of the polluted event. Taking Case-1 as an example, Fig. 3g depicts the evolution of inversion layer. It can be seen that the inversion layer was gradually enhanced from 23 to 27 November but quickly depressed on 28 November, which verifies the results of Fig. 3a–f. Fig. 3h illustrates the distribution of PBLH, which is simulated with the Weather Research & Forecasting (WRF) Model (Zheng et al., 2015c). In Fig. 3h, the PBLH for Case-1 gradually decreased and reached its minimum on the night of 26–27 November. Then the PBLH redeveloped to higher than 1,300 m during the daytime of 28 November. Besides, an ambience with high relative humidity (RH) is favorable for the increase of $PM_{2.5}$ concentration in the ABL through secondary formation by heterogeneous reactions (Quan et al., 2015; Wang et al., 2012; Faust et al., 2017) and hygroscopic growth (Engelhart et al., 2011; Petters and Kreidenweis, 2008). For Case-1, the RH during the CS keeps high with a mean value of 53% but sharply falls into a very low level once entering the TS. Similar results can be found in Case-2.

During CSs, both horizontal wind and vertical wind are weak, implying unfavorable transport conditions. On the contrary, the strength of horizontal and vertical wind notably increases during TSs. These results are consistent with that of u_*, showing a total vertical momentum flux with a mean of 0.25 m s^{-1} during the CS of Case-1 (0.19 and 0.29 m s^{-1} for Case-2). While the values of u_* are generally larger than 0.30 m s^{-1} in the TS of both two cases. According to the classic TKE budget equation (Eq. 5.2.3 in Stull, 1988), the TKE is distinctively produced by the mechanical wind shear near the surface in the TS, resulting in strong turbulent mixing in the ABL, thus more effective transport of air pollutants. Another important term in the TKE budget equation is the buoyant production or consumption. The stability parameter z/L is used here to quantify

the stratification of layers near the surface. Although the values of z/L are negative during the daytime, nocturnal z/L during the CS is notably larger than 1, which means that the consumption caused by buoyancy is dominant compared with the weak production by wind shear. The strongly stable stratification near the surface restrains the vertical turbulence mixing. The reduced mixing, together with emissions and production of secondary pollutants, result in a heavily polluted layer near the surface.

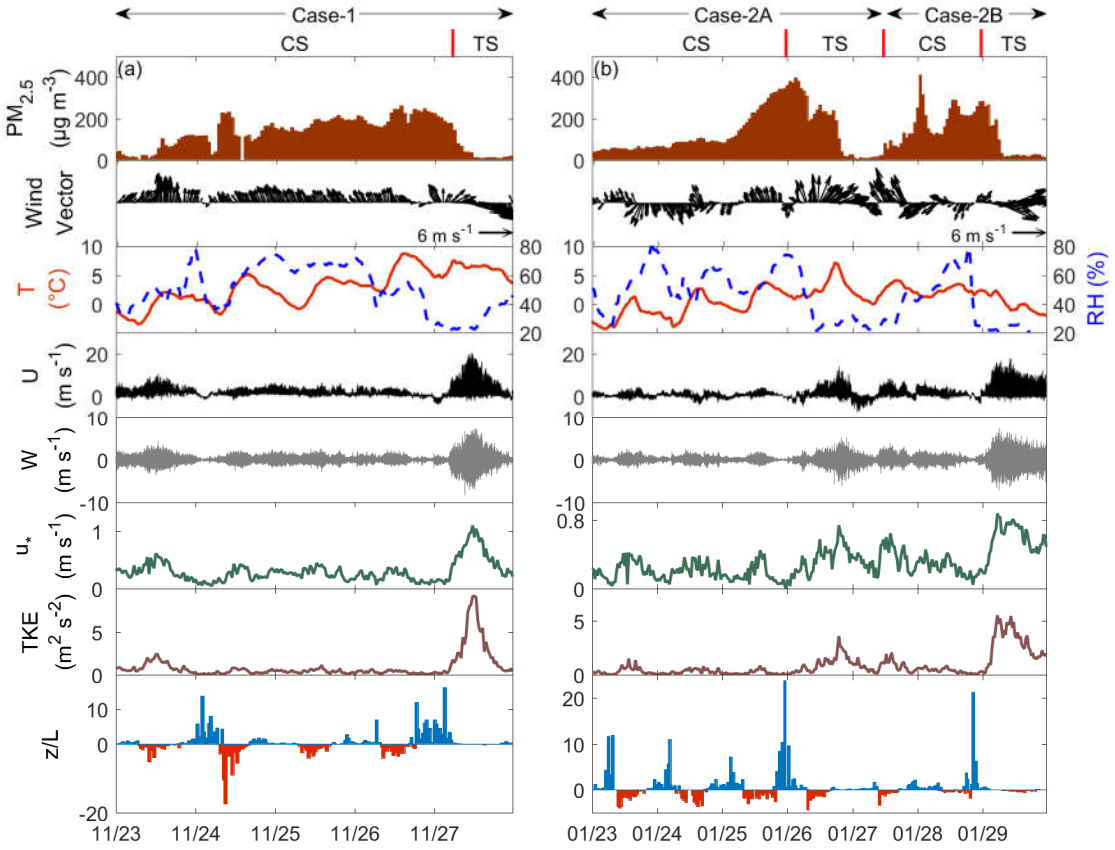

Figure 2. Time series of surface $PM_{2.5}$, wind vector, temperature (T), relative humidity (RH), horizontal wind speed (U), vertical wind speed (W), friction velocity (u_*), turbulent kinetic energy (TKE), and stability parameter (z/L) for Case-1 in (a); for Case-2 in (b). The CS refers to the stage during which pollutants culminated and the TS represents clear days. All of the variables were observed at 40 m except for $PM_{2.5}$ concentration which is at the surface.

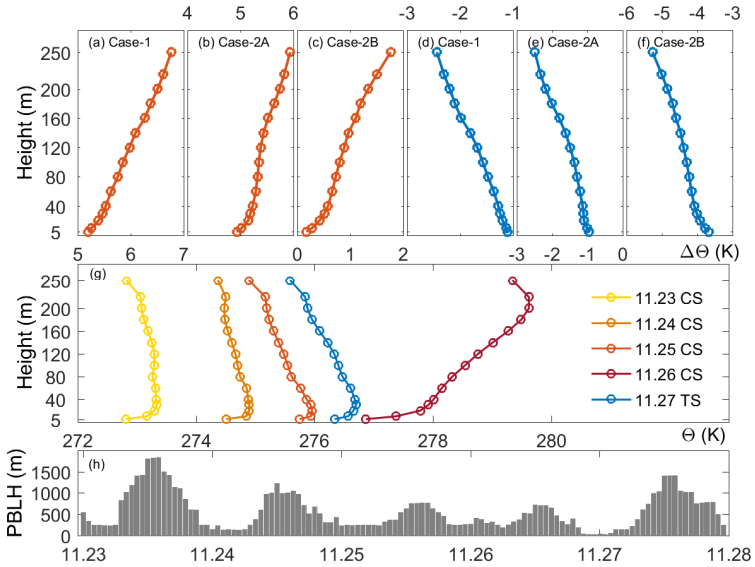

Figure 3. Vertical distribution of daily mean potential temperature. The change of daily mean potential temperature of CSs is showed in (a) – (c) and (d) – (f) are for TSs. (g) illustrates the evolution of inversion layer of Case-1. (h) is the PBLH simulated with WRF Model.

Table 2. Mean and standard deviation (Mean ± SD) of key variables during different periods

Variables	CS	TS	CS	TS
	Case-1		Case-2	
$PM_{2.5}$ (μg m^{-3})	145 ± 71	31 ± 35	139 ± 101 179 ± 85	104 ± 138 75 ± 92
Temperature (K)	275.6 ± 2.9	279.2 ± 0.9	272.7 ± 2.3 275.6 ± 0.8	275.4 ± 1.8 273.1 ± 1.4
RH (%)	53 ± 15	32 ± 8	54 ± 12 48 ± 15	35 ± 17 22 ± 2
U (m s^{-1})	1.85 ± 1.38	3.78 ± 2.90	0.61 ± 0.87 0.67 ± 2.03	1.47 ± 1.39 3.23 ± 1.98
Magnitude of W (m s^{-1})	0.28 ± 0.26	0.61 ± 0.64	0.23 ± 0.22 0.29 ± 0.29	0.36± 0.35 0.62 ± 0.58
u_* (m s^{-1})	0.25 ± 0.12	0.59 ± 0.26	0.19 ± 0.10 0.29 ± 0.13	0.33 ± 0.15 0.58 ± 0.18
TKE (m^2 s^{-2})	0.50 ± 0.43	3.35 ± 2.81	0.28 ± 0.93 0.25 ± 0.71	0.54 ± 0.42 2.87 ± 1.50
z/L at night	1.70 ± 2.74	0.23 ± 0.21	2.18 ± 3.74	0.61 ± 1.43

	1.36 ± 3.31	0.15 ± 0.21

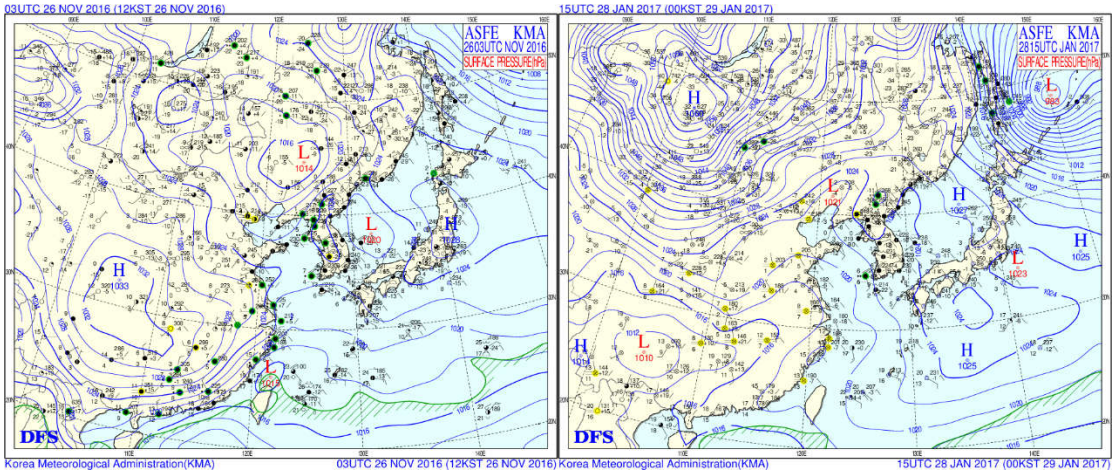

Figure 4. Typical surface weather condition during CSs. Weather charts are from Korea Meteorological Administration.

In addition to the meteorological parameters, synoptic weather conditions also play an important role in the formation and dissipation of heavy air pollutions (Zheng et al., 2015a). Fig. 4 takes two examples from Case-1 and Case-2 to illustrate the typical synoptic weather condition during CSs. In general, the accumulation of pollutants is accompanied by a low pressure system dominating the northern China. Under the control of cyclone system, this region is covered by sparse isobars and is controlled by stagnant wind field, resulting in unfavorable transport conditions.

3.2 Characteristics of intermittent turbulence

Considering the nonlinear and non-stationary nature of turbulent intermittency, it is imperative to choose an effective and reliable method before we implement the analyses. The arbitrary-order HSA used in this work to identify IF index meets the necessary conditions for the analyses of nonlinear and non-stationary time series, such as complete, orthogonal, local, and adaptive (Huang et al., 1998). Our previous works (Wei et al., 2016, 2017) have confirmed the validity of arbitrary-order HSA method in the identification of turbulent intermittency in the ABL.

As mentioned in Sect. 2.2, if turbulence in the ABL is fully developed, the Hilbert-based exponent scaling function $\xi(q)$ should follow the linear distribution of $\xi(q) - 1 = q/3$ (Huang et al., 2008). However, in the real world, there exit all kinds of instability mechanisms on different scales, such as the large-scale baroclinic instability and the small-scale convective instability (Frisch, 1980). Furthermore, under stable conditions, the very low boundary-layer height limit the development of eddies and the stagnant wind near the surface is not enough to maintain the turbulence mixing. Any of these mechanisms would destroy the statistical symmetries stored in the fully developed turbulence, resulting in deviations from K41's q/3 and

a set of concave curves in which the degree of the discrepancy of concave curves manifests the strength of turbulent intermittency. Figs. 5a–5d present the behavior of $\xi(q) - 1$ at 40 m during different stages from two cases. Compared with the theoretical $q/3$, $\xi(q) - 1$ from CSs and TSs both shows deviations to some extent. However, the difference for TSs is much more obvious (in Figs. 5b and 5d), indicating stronger intermittency in the turbulence. Fig. 5e further gives a two-hour example of vertical wind speed during 23:00 on 25 January to 01:00 and 26 January 2017, which covers the transition from the CS to TS in Case-2A. One noticeable feature is that the magnitude of vertical wind fluctuation significantly increases and is marked by strong burst lasting for nearly 25 min from 00:20 to 00:45 on 26 January 2017. On the contrary, the vertical wind speed is relatively weak and steady during the CS. But it should be kept in mind that the small deviations during CSs do not manifest fully developed turbulence but result from the very weak wind speed in the ABL, at which point the wind shear is either absent or not strong enough to generate intermittency (Van de Wiel et al., 2003). The magnitude of vertical wind speed for CSs is generally less than 0.58 m s^{-1}. Under extremely stable conditions, the size of eddies may be too small to be detected by sonic anemometers (Mahrt, 2014).

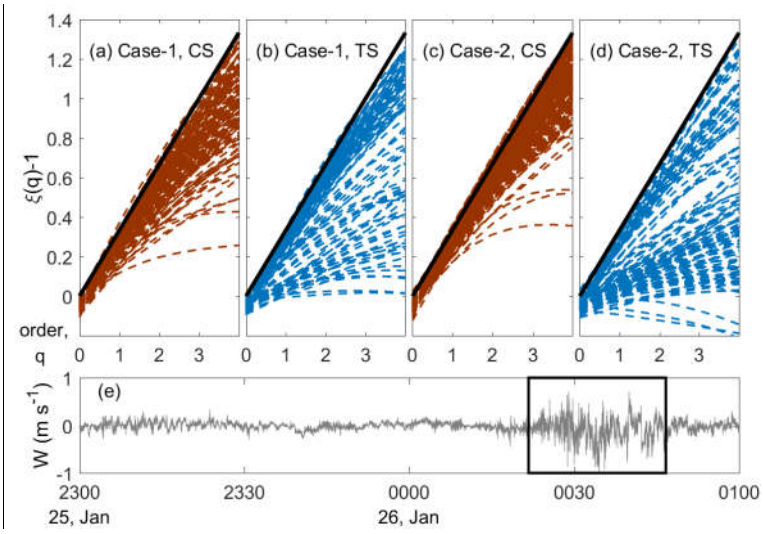

Figure 5. Hilbert-based scaling exponent function at 40 m during different stages for (a) – (b) Case-1 and (c) – (d) Case-2, where each dashed curve represents the result of 30-min vertical wind speed signal and the black solid line denotes the K41 result $q/3$. (e) compares vertical wind fluctuation at 40 m between the CS (before 00:00 on 26 January 2017) and TS (after 00:00 on 26 January 2017). The latter shows apparent 'bursts' marked by the rectangular frame.

In order to measure the strength of turbulent intermittency at different levels, an index named as IF was proposed by this work. Since IF is defined as the deviation from the theoretical $q/3$ at the maximal order q_{max} (here q_{max} equal to 4, see Sect. 2.2), the larger absolute values of IF indicate stronger turbulent intermittency at given height. Meanwhile, time with magnitude of vertical wind speed at 40 m less than 0.3 m s^{-1} is marked to exclude stagnant wind. Fig. 6 illustrates the distribution of IF at three levels, compared with the concentration of $PM_{2.5}$ at the surface. Each sharp decline of surface

$PM_{2.5}$ concentration is accompanied by the abrupt change in values of IF. And IF at 40 m level is especially in agreement with the accumulation and dissipation of pollutants at the surface. The increasing deviations of IF when entering the TS manifest more intermittent turbulence, thus stronger vertical mixing in the ABL. In order to validate the results of IF, another two parameters to indicate the intermittency of turbulence were developed using the same data: one is kurtosis (Vindel et al., 2008) and the other is FI (Mahrt, 1998; Ha et al., 2007). The results of both kurtosis and FI are consistent with those of IF (see Figure ~~S7~~S8–9). In terms of the horizontal wind speed, the 40-m weak wind less than the threshold value (i.e. 5 m s^{-1}) proposed by Van de Wiel et al. (2012) implies that continuous turbulence is unlikely to occur near the surface (Figure S10–11), which corresponds to the very stable turbulence regime-1 or regime-3 in Sun et al. (2012). Previous field results indicate that a significant proportion of vertical fluxes of heat, momentum, and mass under stable conditions come from intermittent bursts (Poulos et al., 2002). Fig. 7 further confirms the relationship between IF and u_* or z/L, in which dots of strong turbulence (u_*) and weak stable stratification ($z/L \approx 0.1$) mainly come from the TS. Larger deviation of IF occurs accompanied by increasing turbulent strength when stability in the ABL becomes weaker. That is, intermittent turbulence (marked by large negative values of IF) leads to strong fluxes during the TS. The enhanced turbulent mixing caused by intermittent bursts contributes positively to the vertical transport of pollutants, improving the air quality near the surface. Besides, the points of intersection from the least-squares regression in Fig. 7 could denote the threshold beyond which the intermittency of turbulence arises under the mutual influence of dynamic and thermodynamic. The values of IF are -0.52 and -0.50 for Case-1 and Case-2, respectively. Hence, a cut-off value of IF (-0.50) can be identified to manifest the significant intermittency of turbulence. But it should be kept in mind that the absolute values of IF change from different heights and sites and this cut-off value of IF can only be used as a reference in the present study.

Besides, another feature of IF in Fig. 6 is that the occurrence of abruptly changed IF at different heights is not simultaneous. In general, the higher the level is, the earlier the intermittent turbulence happens and also the greater the deviations of IF are, which implies that the intermittent turbulence is generated at higher levels and then transported downward. We know that, under weakly stable conditions, turbulence in the ABL is continuous in both time and space, which is mainly dominated by wind shear at the surface. But for strongly stable cases, buoyancy prohibits the turbulent mixing, which enhances the surface radiative cooling, thus increasing the stratification of the ABL (Derbyshire, 1999). Such a positive feedback ultimately leads to the decoupling of boundary layer from the underlying surface, that is, the strong stratification prevents the turbulent exchange between the surface and the ABL. This decoupling could be ceased if there exists wind shear above the stable surface layer, at which point turbulence may be generated at upper levels and then transported downward to rebuild the coupling between the atmosphere and the surface (Mahrt, 1999). The decoupling is suddenly interrupted by the descending turbulence, resulting in intermittent bursts near the surface (Van de Wiel et al., 2012). It is reported (Smedman et al., 1995) that this downward transport of turbulence is related to the pressure transport term in the TKE equation, which means that Monin-Obukhov similarity theory is invalid for this case.

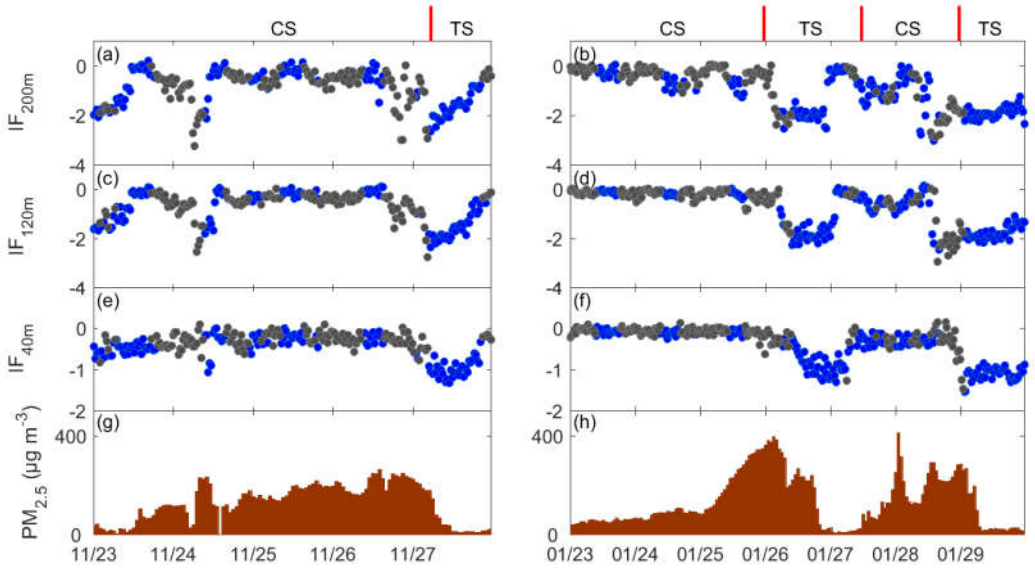

Figure 6. Distribution of (a) – (f) IF at three levels and (g) – (h) concentration of PM2.5 at the surface. Left panel represents Case-1 and right panel for Case-2. Grey dots denote stagnant wind with vertical wind speed less than 0.3 m s^{-1}.

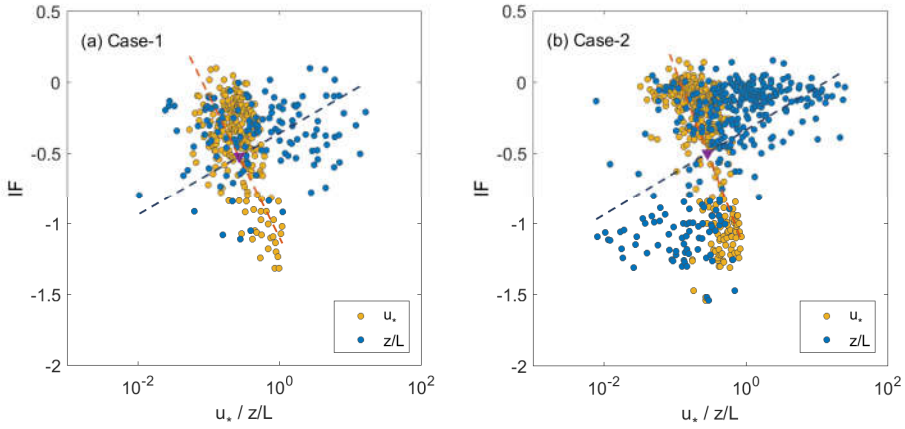

Figure 7. Scatter plot of IF vs. u_* and z/L (night time) for (a) Case-1 and (b) Case-2 at 40 m. The dashed lines are the fittings from least-squares regression and the triangle marks the cross point.

3.3 Mechanism and transport of intermittency

The reasons for intermittent turbulence in the ABL have not yet been well understood. Some potential causes include gravity waves (Sorbjan and Czerwinska, 2013; Strang and Fernado, 2001), solitary waves (Terradellas et al., 2005), horizontal meandering of the mean wind field (Anfossi et al., 2005), and low-level jets (LLJs, Marht, 2014; Banta et al., 2007; 2006; 2003).

According to the case overview in Sect. 3.1, it can be seen that the stratification of surface layers at night is fairly stable during CSs with values of $z/L \gg 1$. Meanwhile, weak u_* and TKE favor the accumulation of pollutants near the surface. In the case of decoupling, it is hard to generate turbulence through the interaction between the atmosphere and the surface. To detect the main sources of turbulence, Fig. 8 presents the height–time cross-section of horizontal wind speed under 2,000 m. The lowest height range of WPR is at 200 m below which observations are seriously interfered by the hard-target returns of around buildings or trees. From Fig. 8a, strong wind occurs at night of 26 November 2016 with maximal wind speed larger than 15 m s^{-1}. For Case-2, there is also strong wind happening in the ABL right before the transitions between the CS and TS (Fig. 8b). After detecting the horizontal wind field, we found that the strong wind in the ABL is generally associated with the happening of LLJs. Fig. 9 takes three profiles as examples to illustrate the LLJ in the ABL. It is well-known that LLJs are an important source of intermittent turbulence in the ABL, resulting in an 'upside-down' boundary layer structure (Mahrt, 1999; 2014; Poulos et al., 2002; Mahrt and Vickers, 2002; Banta et al., 2006; Balsley et al., 2003; Karipot et al., 2008). The vertical 'nose' shape of LLJs provides wind shear at upper levels, working as an elevated source of turbulent mixing. Then this turbulence is transported downward to the surface, resulting in non-stationary increase of turbulent mixing at lower levels. In this case, the vertical structure of 'upside-down' boundary layer is totally different from that of a traditional boundary layer. For example, (a) the wind shear decreases with height first and then increases again due to the LLJ 'nose' at upper levels; (b) the strongest turbulence is not at the surface but aloft; (c) the transport of turbulence energy is downward. Fig. 10 presents the vertical turbulence structure across the tower layer for three dissipation nights, during which LLJs occurred. From Fig. 10a–b, it can be seen that the wind shear weakens in the layer between 40 and 120 m; then it increases when it comes to higher levels. In terms of the variance of vertical wind speed σ_w^2 (Fig. 10d–f), the maximal value of turbulence strength is aloft rather than near the surface for all three nights, implying a turbulence source in mid-air. The vertical distribution of transport of turbulence energy further confirms the uplift of turbulence source. The values of the vertical transport of vertical velocity variance $\overline{w'^3}$ at three levels are negative generally, which means that the transport of turbulence energy across the tower layer is downward. It should be noticed that the magnitude of $\overline{w'^3}$ in Fig. 10h is not monotonously with height, implying a divergence layer of the downward transport of turbulence energy between 120 m and the top of the tower, which suggests that this layer corresponds to the main source of the turbulence in the subjet layer (Mahrt and Vickers, 2002). In addition, ~~T~~the differences in phase and strength of intermittency at three levels in Fig. 6 also ~~indicate~~confirms that the wind shear associated with the LLJ 'nose' ~~may~~ plays an important part in the generation and transport of turbulence in the ABL. Previous study (Wei et al., 2014) has revealed that the LLJ is a common phenomenon in Tianjin region, due to the combined

effects of plain terrain for inertial oscillation (Lundquist, 2003) and strong baroclinicity related to the land–sea temperature contrast offshore (Parish, 2000). In addition, the reduced convection in winter is helpful to maintain the LLJs even during the daytime. In a word, the frequent LLJs in Tianjin region ~~may be~~are a key factor to understand the mechanisms of intermittent turbulence.

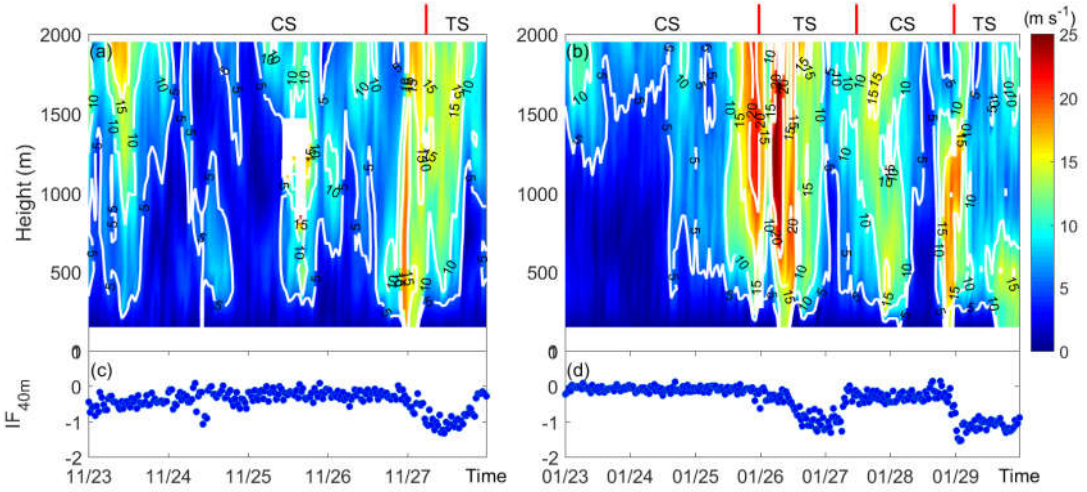

Figure 8. Height–time cross-section of horizontal wind speed observed by WPR for (a) Case-1 and (b) Case-2. (c) – (d) present the corresponding IF at 40 m.

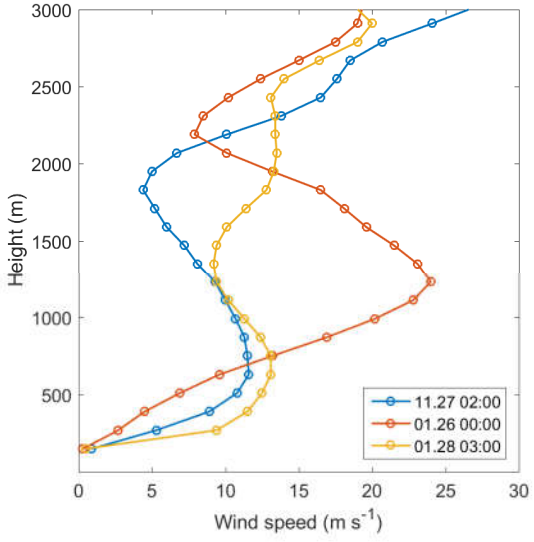

Figure 9. Sample LLJ profiles for three transitions between CSs and TSs.

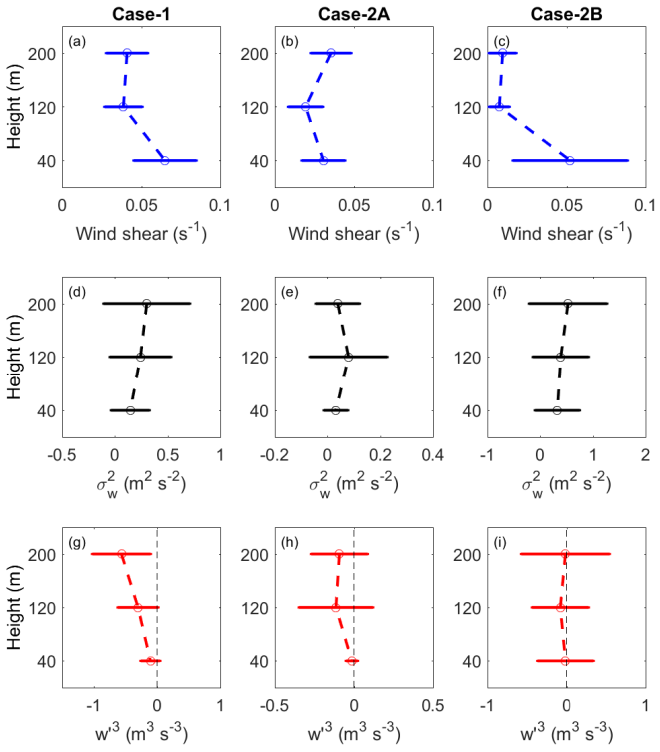

Figure 10. Vertical structure of (a)–(c) Wind shear, (d)–(f) variance of vertical wind speed σ_w^2, (g)–(i) vertical transport of vertical velocity variance $\overline{w'^3}$ during (left) 00:00–00:06 LS on 27, Dec, 2016; (center) 00:00–00:06 LS on 26, Jan, 2017; (right) 00:00–00:06 LS on 29, Jan, 2017. The circle of errorbar denotes the mean value and the width of bar means the standard deviation.

Finally, we summarize the mechanism of intermittent turbulence affecting the $PM_{2.5}$ concentration near the surface in a schematic figure in Fig. ~~10~~11. In the beginning, the inversion layer near the surface enhances due to some favorable conditions including steady synoptic systems, stagnant wind, high temperature and high RH, which leads to the gradual accumulation of particles in the lower boundary layer. Such a process is named as the cumulative stage or CS, during which the turbulence near the surface is too weak to transport pollutants upward. In this case, if there existed LLJs (or other motions) in the ABL, the turbulence could be generated by the strong wind shear associated with the LLJs and then transport downward, resulting in intermittent turbulence at lower levels. The suddenly increased vertical mixing is helpful for the abrupt dissipation of $PM_{2.5}$ near the surface.

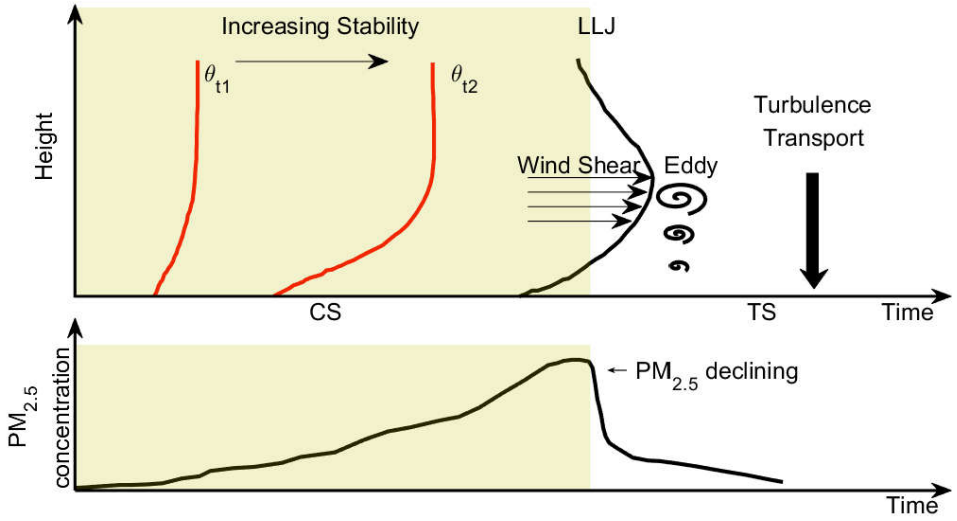

Figure ~~10~~11. Schematic of how intermittent turbulence affects the dissipation of $PM_{2.5}$ near the surface.

4 Conclusion

In the winter of 2016–2017, severe air pollution events haunted the North China Plain. Extremely high concentration of $PM_{2.5}$ threatens the health of the large population living in this region. In this work, two cases in Tianjin (39.00°N, 117.43°E), China were drawn upon to study the effects of intermittent turbulence on the improvement of air quality near the surface. Observations from a 255-m tower, a CFL-03 WPR and a TEOM 1405-DF system were analyzed to investigate the features of boundary-layer structure and $PM_{2.5}$ concentration. In order to measure the levels of turbulent intermittency, an index, called IF, was proposed based on the arbitrary-order HSA which is more suitable for the analyses of nonlinear and non-stationary signals.

At first, ~~due to the absorbed solar radiation by upper air pollutants and the reduced loss of surface longwave outgoing radiation,~~ the inversion layer ~~enhances with stronger heating of upper air layers~~deepens with time. The stability function z/L keeps at high values (>> 1) at night and the stagnant wind field impedes the transport of pollutants. Additionally, high RH and steady cyclone system further aggravate the air pollution. All these factors result in the accumulation of pollutants near the surface.

On the other hand, the concentration of $PM_{2.5}$ undergoes rapid decrease during the dissipation periods, dropping from more than 250 μg m^{-3} to less than 50 μg m^{-3} within a few hours. The dispersion of pollutants coincides with the enhanced turbulent mixing in the ABL. The mean values of u_* and TKE rise to 2–9 times those of the polluted periods. The Hilbert-based exponent scaling function $\xi(q)$ shows great deviations from K41's theoretical result of $q/3$ by a set of concave curves,

indicating that the enhanced turbulence in the ABL when entering the TS is intermittent rather than continuous or fully developed. Using the IF index derived from the vertical wind speed, the abrupt change in IF at 40 m is in agreement with the sharp drop of $PM_{2.5}$ concentration. In addition, the occurrence and strength of intermittent turbulence differ with observation levels. In short, the higher the level is, the earlier the turbulence happens and the stronger the intermittency is, which implies that turbulence is mainly generated at upper levels and then transported to the surface. For 40 m, a cut-off value of IF (-0.50) indicates the initiation of strong turbulent intermittency in the ABL, while this is not a universal value and the threshold varies with different cases.

From the observation of WPR, LLJs were detected right before the dispersion of $PM_{2.5}$. Previous work (Marht, 2014) has pointed out that the stronger wind shear at the height of LLJ 'nose' can be a source of turbulence under the condition of decoupling between the atmosphere and the surface. In this work, LLJs play a key role in the generation of upper-level turbulence. The subsequent downward transport of turbulence leads to intermittent mixing near the surface, thus enhancing the vertical dispersion of $PM_{2.5}$ and improving the air quality.

Data availability. Data used in this study are available from the corresponding author upon request (hsdq@pku.edu.cn).

Competing interests. The authors declare that they have no conflict of interest.

Acknowledgement. This work was jointly funded by grant from National Key R&D Program of China (2016YFC0203300), the National Natural Science Foundation of China (91544216, 41705003, 41475007, 41675018). We also thank Dr. Gao Shanhong at Ocean University of China for providing historical weather-condition charts. Many thanks to Sr. Engr. Yao Qing and Liu Jinle at Tianjin Municipal Meteorological Bureau for their help with the data observation.

References

Anfossi, D., Oettl, D., Degrazia, G. and Goulart, A.: An analysis of sonic anemometer observations in low wind speed conditions, Boundary-Layer Meteorol., 114(1), 179–203, doi:10.1007/s10546-004-1984-4, 2005.

Balsley, B.B., Frehlich, R.G., Jensen, M.L., Meillier, Y. and Muschinski, A.: Extreme gradients in the nocturnal boundary layer: Structure, evolution, and potential causes. J. Atmos. Sci., 60(20), 2496-2508, doi: 10.1175/1520-0469(2003)060<2496:egitnb>2.0.co;2, 2003.

Banta, R. M., Mahrt, L., Vickers, D., Sun, J., Balsley, B. B., Pichugina, Y. L. and Williams, E. J.: The very stable boundary layer on nights with weak low-level jets, J. Atmos. Sci., 64(9), 3068-3090, doi: 10.1175/jas4002.1, 2007.

Banta, R. M., Pichugina, Y. L. and Brewer, W. A.: Turbulent Velocity-Variance Profiles in the Stable Boundary Layer Generated by a Nocturnal Low-Level Jet, J. Atmos. Sci., 63(11), 2700–2719, doi:10.1175/JAS3776.1, 2006.

Banta, R. M., Pichugina, Y. L. and Newsom, R. K.: Relationship between low-level jet properties and turbulence kinetic energy in the nocturnal stable boundary layer, J. Atmos. Sci., 60(20), 2549-2555, doi: 10.1175/1520-0469(2003)060<2549:rbljpa>2.0.co;2, 2003.

Basu, S., Foufoula-Georgiou, E. and Porté-Agel, F.: Synthetic turbulence, fractal interpolation, and large-eddy simulation, Phys. Rev. E, 70(2), 26310, doi:10.1103/PhysRevE.70.026310, 2004.

Bressi, M., Sciare, J., Ghersi, V., Bonnaire, N., Nicolas, J. B., Petit, J. E., Moukhtar, S., Rosso, A., Mihalopoulos, N. and Féron, A.: A one-year comprehensive chemical characterisation of fine aerosol (PM2.5) at urban, suburban and rural background sites in the region of Paris (France), Atmos. Chem. Phys., 13(15), 7825–7844, doi:10.5194/acp-13-7825-2013, 2013.

Chan, C. K. and Yao, X.: Air pollution in mega cities in China, Atmos. Environ., 42, 1–42, doi: 10.1016/j.atmosenv.2007.09.003, 2008.

Cohen, L.: Time-frequency analysis, Prentice Hall, Englewood Cliffs, NJ, 1995.

Derbyshire, S. H.: Boundary-layer decoupling over cold surfaces as a physical boundary-instability, Boundary-Layer Meteorol., 90(2), 297–325, doi:10.1023/A:1001710014316, 1999.

Dominici, F., Greenstone, M. and Sunstein, C. R.: Particulate Matter Matters, Science, 344(6181), 257–259, doi: 10.1126/science.1247348, 2014.

Engelhart, G. J., Hildebrandt, L., Kostenidou, E., Mihalopoulos, N., Donahue, N. M. and Pandis, S. N.: Water content of aged aerosol, Atmos. Chem. Phys., 11(3), 911–920, doi:10.5194/acp-11-911-2011, 2011.

Faust, J. A., Wong, J. P. S., Lee, A. K. Y., and Abbatt, J. P.: Role of Aerosol Liquid Water in Secondary Organic Aerosol Formation from Volatile Organic Compounds, Environ. Sci. Techmol., 51(3): 1405-1413, doi: 10.1021/acs.est.6b04700, 2017.

Frisch, U.: Fully developed turbulence and intermittency, Ann. NY. Acad. Sci., 357(1): 359-367, doi: 10.1111/j.1749-6632.1980.tb29703.x, 1980.

Frisch, U.: Turbulence: the legacy of AN Kolmogorov, Cambridge university press, Great Britain, 1995.

Gao, S., Wang, Y., Huang, Y., Zhou, Q., Lu, Z., Shi, X. and Liu, Y.: Spatial statistics of atmospheric particulate matter in China, Atmos. Environ., 134, 162–167, doi:10.1016/j.atmosenv.2016.03.052, 2016.

Ha, K. J., Hyun, Y. K., Oh, H. M., Kim, K. E. and Mahrt, L.: Evaluation of boundary layer similarity theory for stable conditions in CASES-99, Mon. Weather Rev., 135(10), 3474-3483, doi: 10.1007/bf00119423, 2007.

Helgason, W. and Pomeroy, J. W.: Characteristics of the near-surface boundary layer within a mountain valley during winter, J. Appl. Meteorol. Climatol., 51(3), 583–597, doi:10.1175/JAMC-D-11-058.1, 2012.

Holtslag, A. A. M.: BOUNDARY LAYER (ATMOSPHERIC) AND AIR POLLUTION | Modeling and Parameterization, in Encyclopedia of Atmospheric Sciences, vol. 1, pp. 265–273, Elsevier., 2015.

Huang, N., Shen, Z., Long, S., Wu, M., Shih, H., Zheng, Q., Yen, N., Tung, C. and Liu, H.: The empirical mode decomposition and the Hilbert spectrum for nonlinear and non-stationary time series analysis, Proc. R. Soc. A Math. Phys. Eng. Sci., 454(1971), 903–995, doi:10.1098/rspa.1998.0193, 1998.

Huang, N. E., Shen, Z. and Long, S. R.: A new view of nonlinear water waves: the Hilbert Spectrum, Annu. Rev. Fluid Mech., 31(1), 417–457, doi:10.1146/annurev.fluid.31.1.417, 1999.

Huang, Y., Schmitt, F. G., Lu, Z. and Liu, Y.: Analysis of daily river flow fluctuations using empirical mode decomposition and arbitrary order Hilbert spectral analysis, J. Hydrol., 373(1–2), 103–111, doi:10.1016/j.jhydrol.2009.04.015, 2009.

Huang, Y. X., Schmitt, F. G., Lu, Z. M. and Liu, Y. L.: An amplitude-frequency study of turbulent scaling intermittency using Empirical Mode Decomposition and Hilbert Spectral Analysis, EPL (Europhysics Lett., 84(4), 40010, doi:10.1209/0295-5075/84/40010, 2008.

Huang, Y. X., Schmitt, F. G., Hermand, J. P., Gagne, Y., Lu, Z. M. and Liu, Y. L.: Arbitrary-order Hilbert spectral analysis for time series possessing scaling statistics: Comparison study with detrended fluctuation analysis and wavelet leaders, Phys. Rev. E, 84(1), 16208, doi:10.1103/PhysRevE.84.016208, 2011.

Jiang, C., Wang, H., Zhao, T., Li, T., and Che, H.: Modeling study of PM 2.5 pollutant transport across cities in China's Jing–Jin–Ji region during a severe haze episode in December 2013, Atmos. Chem. Phys., 15(10), 5803-5814, doi: 10.5194/acpd-15-3745-2015, 2015.

Karipot, A., Leclerc, M.Y., Zhang, G., Lewin, K.F., Nagy, J., Hendrey, G.R. and Starr, G.: Influence of nocturnal low-level jet on turbulence structure and CO2 flux measurements over a forest canopy, J. Geophys. Res.-Atmos., 113(D10), doi: 10.1029/2007jd009149, 2008.

Klipp, C. L. and Mahrt, L.: Flux-gradient relationship, self-correlation and intermittency in the stable boundary layer, Q. J. R. Meteorol. Soc., 130(601), 2087–2103, doi:10.1256/qj.03.161, 2004.

Lundquist, J. K.: Intermittent and Elliptical Inertial Oscillations in the Atmospheric Boundary Layer, J. Atmos. Sci., 60(1997), 2661–2673, doi:10.1175/1520-0469(2003)060<2661:IAEIOI>2.0.CO;2, 2003.

Mahrt, L.: Nocturnal Boundary-Layer Regimes, Boundary-layer Meteorol., 88(2), 255–278, doi:10.1023/A:1001171313493, 1998.

Mahrt, L.: Stratified Atmospheric Boundary Layers, Boundary-Layer Meteorol., 90(3), 375–396, doi:10.1023/A:1001765727956, 1999.

Mahrt, L.: Stably Stratified Atmospheric Boundary Layers, Annu. Rev. Fluid Mech., 46, 23–45, doi:10.1146/annurev-fluid-010313-141354, 2014.

Miao, Y., Guo, J., Liu, S., Liu, H., Zhang, G., Yan, Y. and He, J.: Relay transport of aerosols to Beijing-Tianjin-Hebei region by multi-scale atmospheric circulations, Atmos. Environ., 165, 35–45, doi:10.1016/j.atmosenv.2017.06.032, 2017.

Nel, A.: ATMOSPHERE: Enhanced: Air Pollution-Related Illness: Effects of Particles, Science, 308(5723), 804–806, doi:10.1126/science.1108752, 2005.

Noone, D., Risi, C., Bailey, A., Berkelhammer, M., Brown, D. P., Buenning, N., Gregory, S., Nusbaumer, J., Schneider, D., Sykes, J., Vanderwende, B., Wong, J., Meillier, Y. and Wolfe, D.: Determining water sources in the boundary layer from tall tower profiles of water vapor and surface water isotope ratios after a snowstorm in Colorado, Atmos. Chem. Phys., 13(3), 1607–1623, doi:10.5194/acp-13-1607-2013, 2013.

Parish, T. R.: Forcing of the Summertime Low-Level Jet along the California Coast, J. Appl. Meteorol., 39(12), 2421–2433, doi:10.1175/1520-0450(2000)039<2421:FOTSLL>2.0.CO;2, 2000.

Petäjä, T., Järvi, L., Kerminen, V. M., Ding, A. J., Sun, J. N., Nie, W., Kujansuu, J., Virkkula, A., Yang, X., Fu, C. B., Zilitinkevich, S. and Kulmala, M.: Enhanced air pollution via aerosol-boundary layer feedback in China, Sci. Rep., 6(January), doi:10.1038/srep18998, 2016.

Petters, M. D. and Kreidenweis, S. M.: A single parameter representation of hygroscopic growth and cloud condensation nucleus activity – Part 2: Including solubility, Atmos. Chem. Phys. Discuss., 8(2), 5939–5955, doi:10.5194/acpd-8-5939-2008, 2008.

Poulos, G. S., Blumen, W., Fritts, D. C., Lundquist, J. K., Sun, J., Burns, S. P., Nappo, C., Banta, R., Newsom, R., Cuxart, J., Terradellas, E., Balsley, B. and Jensen, M.: CASES-99: A comprehensive investigation of the stable nocturnal boundary layer, Bull. Am. Meteorol. Soc., 83(4), 555–581, doi:10.1175/1520-0477(2002)083<0555:CACIOT>2.3.CO;2, 2002.

Quan, J., Liu, Q., Li, X., Gao, Y., Jia, X., Sheng, J. and Liu, Y.: Effect of heterogeneous aqueous reactions on the secondary formation of inorganic aerosols during haze events, Atmos. Environ., 122, 306–312, doi:10.1016/j.atmosenv.2015.09.068, 2015.

Ren, Y., Zheng, S., Wei, W., Wu, B., Zhang, H., Cai, X. and Song, Y.: Characteristics of the Turbulent Transfer during the Heavy Haze in Winter 2016 / 17 in Beijing, J. Meteorol. Res., doi:10.1007/s13351-018-7072-3, 2017.

Salmond, J. A.: Wavelet analysis of intermittent turbulence in a very stable nocturnal boundary layer: implications for the vertical mixing of ozone, Boundary-Layer Meteorol., 114(3), 463–488, doi:10.1007/s10546-004-2422-3, 2005.

Schmitt, F. G., Huang, Y., Lu, Z., Liu, Y. and Fernandez, N.: Analysis of velocity fluctuations and their intermittency properties in the surf zone using empirical mode decomposition, J. Mar. Syst., 77(4), 473–481, doi:10.1016/j.jmarsys.2008.11.012, 2009.

Shen, Z., Cui, G. and Zhang, Z.: Turbulent dispersion of pollutants in urban-type canopies under stable stratification conditions, Atmos. Environ., 156, 1–14, doi:10.1016/j.atmosenv.2017.02.017, 2017.

Smedman, A. S., Bergström, H. and Högström, U.: Spectra, variances and length scales in a marine stable boundary layer dominated by a low level jet, Boundary-Layer Meteorol., 76(3), 211–232, doi:10.1007/BF00709352, 1995.

Sorbjan, Z. and Czerwinska, A.: Statistics of Turbulence in the Stable Boundary Layer Affected by Gravity Waves, Boundary-Layer Meteorol., 148(1), 73–91, doi:10.1007/s10546-013-9809-y, 2013.

Strang, E. J. and Fernado, H. J. S.: Entrainment and mixing in stratified shear flows, J. Fluid Mech., 428(6S), 349–386, doi:10.1017/S0022112000002706, 2001.

Stull, R.B.: An Introduction to Boundary Layer Meteorology, Kluwer Academic, USA, 1988.

Sun, J., Mahrt, L., Banta, R.M. and Pichugina, Y.L.: Turbulence regimes and turbulence intermittency in the stable boundary layer during CASES-99, J. Atmos. Sci., 69(1), 338–351, doi: 10.1175/jas-d-11-082.1, 2012.

Sun, J., Mahrt, L., Nappo, C. and Lenschow, D. H.: Wind and Temperature Oscillations Generated by Wave–Turbulence Interactions in the Stably Stratified Boundary Layer, J. Atmos. Sci., 72(4), 1484–1503, doi:10.1175/JAS-D-14-0129.1, 2015.

Sun, Y., Zhuang, G., Wang, Y., Han, L., Guo, J., Dan, M., Zhang, W., Wang, Z. and Hao, Z.: The air-borne particulate pollution in Beijing - Concentration, composition, distribution and sources, Atmos. Environ., 38(35), 5991–6004, doi:10.1016/j.atmosenv.2004.07.009, 2004.

Tang, G., Zhang, J., Zhu, X., Song, T., Münkel, C., Hu, B., Schäfer, K., Liu, Z., Zhang, J., Wang, L., Xin, J., Suppan, P. and Wang, Y.: Mixing layer height and its implications for air pollution over Beijing, China, Atmos. Chem. Phys., 16(4), 2459–2475, doi:10.5194/acp-16-2459-2016, 2016.

Terradellas, E., Soler, M. R., Ferreres, E. and Bravo, M.: Analysis of oscillations in the stable atmospheric boundary layer using wavelet methods, Boundary-Layer Meteorol., 114, 489–518, doi:10.1007/s10546-004-1293-y, 2005.

Thompson, T. M., Saari, R. K. and Selin, N. E.: Air quality resolution for health impact assessment: Influence of regional characteristics, Atmos. Chem. Phys., 14(2), 969–978, doi:10.5194/acp-14-969-2014, 2014.

Vindel, J. M., Yagüe, C. and Redondo, J. M.: Structure function analysis and intermittency in the atmospheric boundary layer, Nonlinear. Proc. Geoph., 15(6), 915-929, doi: 10.5194/npg-15-915-2008, 2008.

Vindel, J. M. and Yagüe, C.: Intermittency of Turbulence in the Atmospheric Boundary Layer: Scaling Exponents and Stratification Influence, Boundary-Layer Meteorol., 140(1), 73–85, doi:10.1007/s10546-011-9597-1, 2011.

Wang, T., Nie, W., Gao, J., Xue, L. K., Gao, X. M., Wang, X. F., Qiu, J., Poon, C. N., Meinardi, S., Blake, D., Wang, S. L., Ding, A. J., Chai, F. H., Zhang, Q. Z. and Wang, W. X.: Air quality during the 2008 Beijing Olympics: Secondary pollutants and regional impact, Atmos. Chem. Phys., 10(16), 7603–7615, doi:10.5194/acp-10-7603-2010, 2010.

Wang, X., Wang, W., Yang, L., Gao, X., Nie, W., Yu, Y., Xu, P., Zhou, Y. and Wang, Z.: The secondary formation of inorganic aerosols in the droplet mode through heterogeneous aqueous reactions under haze conditions, Atmos. Environ., 63, 68–76, doi:10.1016/j.atmosenv.2012.09.029, 2012.

Wang, X., Dickinson, R. E., Su, L., Zhou, C. and Wang, K.: PM 2.5 Pollution in China and How It Has Been Exacerbated by Terrain and Meteorological Conditions, Bull. Am. Meteorol. Soc., doi:10.1175/BAMS-D-16-0301.1, 2017.

Wei, W., Zhang, H. S. and Ye, X. X.: Comparison of low-level jets along the north coast of China in summer, J. Geophys. Res. Atmos., 119(16), 9692–9706, doi:10.1002/2014JD021476, 2014.

Wei, W., Schmitt, F. G., Huang, Y. X. and Zhang, H. S.: The Analyses of Turbulence Characteristics in the Atmospheric Surface Layer Using Arbitrary-Order Hilbert Spectra, Boundary-Layer Meteorol., 159(2), 391–406, doi:10.1007/s10546-015-0122-9, 2016.

Wei, W., Wang, M., Zhang, H., He, Q., Ali, M. and Wang, Y.: Diurnal characteristics of turbulent intermittency in the Taklimakan Desert, Meteorol. Atmos. Phys., doi:10.1007/s00703-017-0572-3, 2017.

Van de Wiel, B. J. H., Moene, a. F., Hartogensis, O. K., De Bruin, H. a. R. and Holtslag, a. a. M.: Intermittent Turbulence in the Stable Boundary Layer over Land. Part III: A Classification for Observations during CASES-99, J. Atmos. Sci., 60(20), 2509–2522, doi:10.1175/1520-0469(2003)060<2509:ITITSB>2.0.CO;2, 2003.

Van de Wiel, B. J. H., Moene, A. F., Jonker, H. J. J., Baas, P., Basu, S., Donda, J. M. M., Sun, J. and Holtslag, A. A. M.: The Minimum Wind Speed for Sustainable Turbulence in the Nocturnal Boundary Layer, J. Atmos. Sci., 69(11), 3116–3127, doi:10.1175/JAS-D-12-0107.1, 2012.

Ye, X., Wu, B. and Zhang, H.: The turbulent structure and transport in fog layers observed over the Tianjin area, Atmos. Res., 153, 217–234, doi:10.1016/j.atmosres.2014.08.003, 2014.

Ye, X., Song, Y., Cai, X. and Zhang, H.: Study on the synoptic flow patterns and boundary layer process of the severe haze events over the North China Plain in January 2013, Atmos. Environ., 124(January 2013), 129–145, doi:10.1016/j.atmosenv.2015.06.011, 2016.

Yin, Z. and Wang, H.: Role of atmospheric circulations in haze pollution in December 2016, Atmos. Chem. Phys., 17(18), 11673–11681, doi:10.5194/acp-17-11673-2017, 2017.

Yin, Z., Wang, H. and Chen, H.: Understanding severe winter haze events in the North China Plain in 2014: Roles of climate anomalies, Atmos. Chem. Phys., 17(3), 1641–1651, doi:10.5194/acp-17-1641-2017, 2017.

Zhang, H., Chen, J. and Park, S.: Turbulence structure in unstable conditions over various surfaces, Boundary-Layer Meteorol., 100(2), 243–261, doi:10.1023/A:1019223316895, 2001.

Zhang, H., Wang, S., Hao, J., Wang, X., Wang, S., Chai, F. and Li, M.: Air pollution and control action in Beijing, J. Clean. Prod., 112, 1519–1527, doi:10.1016/j.jclepro.2015.04.092, 2016.

Zhang, J. P., Zhu, T., Zhang, Q. H., Li, C. C., Shu, H. L., Ying, Y., Dai, Z. P., Wang, X., Liu, X. Y., Liang, A. M., Shen, H. X. and Yi, B. Q.: The impact of circulation patterns on regional transport pathways and air quality over Beijing and its surroundings, Atmos. Chem. Phys., 12(11), 5031–5053, doi:10.5194/acp-12-5031-2012, 2012.

Zhang, Y.-L. and Cao, F.: Fine particulate matter (PM2.5) in China at a city level, Sci. Rep., 5(October), 14884, doi:10.1038/srep14884, 2015.

Zhang, Y., Zhu, B., Gao, J., Kang, H., Yang, P., Wang, L., and Zhang, J: The source apportionment of primary PM2. 5 in an aerosol pollution event over Beijing-Tianjin-Hebei region using WRF-Chem, China, Aerosol Air Qual. Res., 17, 2966-2980, doi: 10.4209/aaqr.2016.10.0442, 2017.

Zheng, G. J., Duan, F. K., Su, H., Ma, Y. L., Cheng, Y., Zheng, B., Zhang, Q., Huang, T., Kimoto, T., Chang, D., Pöschl, U., Cheng, Y. F. and He, K. B.: Exploring the severe winter haze in Beijing: The impact of synoptic weather, regional transport and heterogeneous reactions, Atmos. Chem. Phys., 15(6), 2969–2983, doi:10.5194/acp-15-2969-2015, 2015a.

Zheng, S., Pozzer, A., Cao, C. X. and Lelieveld, J.: Long-term (2001-2012) concentrations of fine particulate matter (PM2.5) and the impact on human health in Beijing, China, Atmos. Chem. Phys., 15(10), 5715–5725, doi:10.5194/acp-15-5715-2015, 2015b.

Zheng, B., Zhang, Q., Zhang, Y., He, K. B., Wang, K., Zheng, G. J.,Duan, F. K., Ma, Y. L., and Kimoto, T.: Heterogeneous chemistry: a mechanism missing in current models to explain secondary inorganic aerosol formation during the January 2013 haze episode in North China, Atmos. Chem. Phys., 15, 2031–2049, doi:10.5194/acp-15-2031-2015, 2015c.

Zhong, J., Zhang, X., Wang, Y., Sun, J., Zhang, Y., Wang, J., Tan, K., Shen, X., Che, H., Zhang, L., Zhang, Z., Qi, X., Zhao, H., Ren, S. and Li, Y.: Relative contributions of boundary-layer meteorological factors to the explosive growth of PM2.5during the red-alert heavy pollution episodes in Beijing in December 2016, J. Meteorol. Res., 31(5), 809–819, doi:10.1007/s13351-017-7088-0, 2017.